NAVAL POSTGRADUATE SCHOOL

MONTEREY, CALIFORNIA

THESIS

DISTRIBUTED BEAMFORMING IN MAN PORTABLE COMMUNICATION NETWORKS

by

Chan, Chun Man

December 2007

Thesis Advisor:	David Jenn
Second Reader:	Murali Tummala

Approved for public release; distribution is unlimited

THIS PAGE INTENTIONALLY LEFT BLANK

REPORT DOCUMENTATION PAGE			*Form Approved OMB No. 0704-0188*
Public reporting burden for this collection of information is estimated to average 1 hour per response, including the time for reviewing instruction, searching existing data sources, gathering and maintaining the data needed, and completing and reviewing the collection of information. Send comments regarding this burden estimate or any other aspect of this collection of information, including suggestions for reducing this burden, to Washington headquarters Services, Directorate for Information Operations and Reports, 1215 Jefferson Davis Highway, Suite 1204, Arlington, VA 22202-4302, and to the Office of Management and Budget, Paperwork Reduction Project (0704-0188) Washington DC 20503.			
1. AGENCY USE ONLY ***(Leave blank)***	**2. REPORT DATE** December 2007	**3. REPORT TYPE AND DATES COVERED** Master's Thesis	
4. TITLE AND SUBTITLE Distributed Beamforming in Man Portable Communication Networks		**5. FUNDING NUMBERS**	
6. AUTHOR(S) Chan, Chun Man			
7. PERFORMING ORGANIZATION NAME(S) AND ADDRESS(ES) Naval Postgraduate School Monterey, CA 93943-5000		**8. PERFORMING ORGANIZATION REPORT NUMBER**	
9. SPONSORING /MONITORING AGENCY NAME(S) AND ADDRESS(ES) N/A		**10. SPONSORING/MONITORING AGENCY REPORT NUMBER**	
11. SUPPLEMENTARY NOTES The views expressed in this thesis are those of the author and do not reflect the official policy or position of the Department of Defense or the U.S. Government.			
12a. DISTRIBUTION / AVAILABILITY STATEMENT Approved for public release; distribution is unlimited		**12b. DISTRIBUTION CODE**	

13. ABSTRACT (maximum 200 words)

The advancement in communication and networking technologies lead to the emergence of network centric systems adopted by military forces. Many military forces around the world are equipping their ground soldiers with "man portable" or "mobile" wireless communication devices to form a local communication network as part of the overarching communication network for information warfare. In a non-line of sight environment, the devices' communication range to the base station degrades significantly.

The research objective is to examine collaborative beamforming man portable wireless communication networks in a non-ideal propagation operation environment such as in a terrain with foliage. Using distributed beamforming techniques with wireless radios, the communication range can be increased to overcome foliage attenuation and other losses. Seasonal foliage effects on the wireless network were considered in the study. Wireless beamforming strategies were devised and an analysis of system performance and tradeoffs was conducted. System synchronization of the wireless collaborative communication network is a major challenge due to the lack of fixed infrastructure and the dynamic topology of the network. Two network synchronization schemes: mutual synchronization and master-slave synchronization were investigated. Finally, an analysis of phase errors, which affect the gains achieved by distributed beamforming, was performed.

14. SUBJECT TERMS Wireless network, distributed beamforming, collaborative beamforming, foliage, synchronization			**15. NUMBER OF PAGES** 117
			16. PRICE CODE
17. SECURITY CLASSIFICATION OF REPORT Unclassified	**18. SECURITY CLASSIFICATION OF THIS PAGE** Unclassified	**19. SECURITY CLASSIFICATION OF ABSTRACT** Unclassified	**20. LIMITATION OF ABSTRACT** UU

NSN 7540-01-280-5500 Standard Form 298 (Rev. 2-89)
Prescribed by ANSI Std. 239-18

THIS PAGE INTENTIONALLY LEFT BLANK

Approved for public release; distribution is unlimited

DISTRIBUTED BEAMFORMING IN MAN PORTABLE COMMUNICATION NETWORKS

Chan, Chun Man
Civilian, Singapore Technologies Kinetics Ltd
Bachelor of Engineering(Hons), University of Manchester Institute of Science and Technology, United Kingdom, 1997

Submitted in partial fulfillment of the
requirements for the degree of

MASTER OF SCIENCE IN ELECTRICAL ENGINEERING

from the

NAVAL POSTGRADUATE SCHOOL
December 2007

Author: Chan, Chun Man

Approved by: David Jenn
Thesis Advisor

Murali Tummala
Second Reader

Jeffrey B. Knorr
Chairman, Department of Electrical and Computer Engineering

THIS PAGE INTENTIONALLY LEFT BLANK

ABSTRACT

The advancement in communication and networking technologies lead to the emergence of network centric systems adopted by military forces. Many military forces around the world are equipping their ground soldiers with “man portable” or “mobile” wireless communication devices to form a local communication network as part of the overarching communication network for information warfare. In a non-line of sight environment, the devices’ communication range to the base station degrades significantly.

The research objective is to examine collaborative beamforming man portable wireless communication networks in a non-ideal propagation operation environment such as in a terrain with foliage. Using distributed beamforming techniques with wireless radios, the communication range can be increased to overcome foliage attenuation and other losses. Seasonal foliage effects on the wireless network were considered in the study. Wireless beamforming strategies were devised and an analysis of system performance and tradeoffs was conducted. System synchronization of the wireless collaborative communication network is a major challenge due to the lack of fixed infrastructure and the dynamic topology of the network. Two network synchronization schemes: mutual synchronization and master-slave synchronization were investigated. Finally, an analysis of phase errors, which affect the gains achieved by distributed beamforming, was performed.

THIS PAGE INTENTIONALLY LEFT BLANK

TABLE OF CONTENTS

THIS PAGE INTENTIONALLY LEFT BLANK

LIST OF FIGURES

THIS PAGE INTENTIONALLY LEFT BLANK

LIST OF TABLES

THIS PAGE INTENTIONALLY LEFT BLANK

EXECUTIVE SUMMARY

Modern day information warfare equips ground soldiers with technologically advanced subsystems such as: health monitoring system, video surveillance system, global positioning system, a computer, and most importantly, a wireless communication system as the heart of the system. The wireless communication system provides connectivity in terms of data and voice between the soldiers and between the soldiers and their vehicle, and through the vehicle communication system to the higher echelon of commands. The soldiers on the ground play the role of mission execution and are paramount to any mission success.

Connectivity in the wireless communication network is therefore vital in modern day information warfare. In a foliage terrain, connectivity distance of the communication system degrades and the network becomes narrower in a non-line of sight environment, decreasing the field operating distance of the soldiers. It is interesting to note that the communication system manufacturer usually only specifies the line of sight distance in its technical specifications. Increasing the connectivity of soldiers on the ground means that the communication network coverage area can be broadened in terms of field operation distance, which could be decisive to a mission success.

The objective of this thesis is the investigation of distributed beamforming in wireless networks. The communication range can be increased to overcome foliage attenuation and other losses. Different Personal Role Radio (PRR) system configurations under field operating scenarios are modeled in Matlab. Two baseline models are used for reference: (1) a link between a single wireless device and a vehicle antenna, and (2) a link between two wireless devices. The results are used as a baseline for comparison with other scenarios. Findings showed that beamforming can be applied for all the specified scenarios with some range improvements realized. However, the small half power beam width means that knowledge of the locations of the PRRs and receiving antenna must be very accurate to focus the beam at the correct location for efficient beamforming and reap the benefit of higher range operations.

A second issue is the seasonal foliage effects on the wireless network in the environment of operation. The foliage environment effects on wave propagation were presented and the rationale, considerations and assumptions on modeling of the seasonal foliage environment were described. The Matlab simulation results showed that the benefits gained from the adopted beamforming strategies cannot completely overcome the effects of the foliage environment due to excess path loss but still show a significant increase in communication range. Improvement on the order of 28.5% and 85% increase in communication range for summer and winter conditions are predicted achievable with beamforming.

While the benefits of beamforming brought about an increase in terms of gains resulting in greater communication range, there is a cost associated with synchronizing the PRR elements in order to achieve these gains. This cost depends not only on accurate knowledge of the channel, but also time and phase synchronization at the transmitter. Two network synchronization schemes: mutual synchronization and master-slave synchronization were investigated. A statistical analysis of phase errors, which affect the gains achieved by distributed beamforming was performed. Results showed that with a uniformly distributed placement error of $\Delta = 8$ (4 wavelengths) and beamforming using 3 PRR elements, there is a 42% loss of expected value of received power and 60% loss for the variance for the received power relative to the error free case. However, the expected value of received power is still 1.7 times and the variance for the received power is still 1.53 times that for a single antenna transmission. For the extreme case of placement error of $\Delta = 8$ with $N = 30$ (maximum number of users), there is a 60% loss of expected value of received power and 75% loss for the variance for the received power. Nevertheless, the expected value of the received power is still 12 times and the variance for the received power is still 8.8 times that of a single antenna transmission.

ACKNOWLEDGMENTS

I would like to express my heartfelt gratitude to my beloved wife, Ann, daughter and son, Josie and Joshua for their love, understanding, trust, and moral support during the preparation of the thesis.

I would also like to express my utmost appreciation to Professor David Jenn for his valuable advice, time and patience throughout the process of this thesis. His understanding, attention, belief and expertise gave me invaluable support in completing this thesis.

My gratitude to Professor Murali Tummala for his time and effort in reviewing the thesis and valuable feedback contributed.

I would also like to thank Mr. Bob Broadston for his willingness to provide Matlab programming advice and being approachable all the time.

Last but not least, my thanks to those who have contributed positively to the completion of the thesis.

THIS PAGE INTENTIONALLY LEFT BLANK

I. INTRODUCTION

A. GENERAL

Many armies around the world are enabling their future soldiers to be lighter, faster and more mobile. Soldiers are equipped with cutting edge technology tools providing increased survivability and lethality through real-time update of mission critical data, allowing clear and concise battlefield situational awareness and faster closure of the sensor to shooter loop in modern information warfare.

Future soldiers are empowered with the ability to transmit and receive voice and data signals, fast processing speed and advanced handheld computing capability such as mapping, navigation and freehand sketching of pre-determined tactical symbols. The advance communication tools turn simple foot soldiers into powerful fighting units readily plugged into the main grid of the digital battlefield.

The heartbeat of the system is known as Personal Role Radio (PRR), usually a short range radio operating independently of any infrastructures. PRRs offer effective communications within the mission operating squad and between combat teams, enabling cohesive dismounted infantry operations. Present PRR systems are functioning in the 2.4 GHz and upper UHF bands, offering effective short range communications with low interference and adequate bandwidth utilization. Most systems operate in duplex conference modes, where the commander can speak to all his soldiers and get their responses, or in selective peer to peer communications which is one to one.

PRRs support only line of sight communications at ranges of few hundred meters. Systems support mainly voice but some can also transfer data at low bit rate, to transmit images, files, reports, etc. As PRRs operate at low power and high frequencies, there are significant constraints in communications during operations in high density deciduous foliage environments. When in a non-line of sight environment, the usual communication ranges of few hundred meters deteriorate to less than a hundred meters, thereby affecting mission execution. PRRs are not maximizing their performance in relation to their designed specification in terms of range. These constraints make the PRRs an excellent

research opportunity for many real life issues. They are especially of interest to the military environment as PRR communications are critical to soldiers executing a mission, which could mean the difference between mission success and failure. Reduced communications can also endanger the soldiers as cohesiveness in mission execution is lost. The PRRs should be able to provide reliable communications at all time for the commander and his soldiers executing missions in different weather conditions and any environment and terrain.

B. THESIS MOTIVATION

The constraints of PRR systems operating in urban or foliage environments are well known to the military commanders from conducting field trials. Where the advantages of employing the PRRs cannot be defaulted, the lack of communications at higher ranges which limits their mission profile while operating in urban or foliage environments (highly likely terrain for their operations) cannot be ignored. Therefore, the commanders are questioning the viability of these PRR systems and the worthiness of equipping their soldiers with such systems [1].

There has also been considerable research done in [2-5] to increase communication ranges by employing distributed beamforming techniques. Using distributed beamforming in wireless networks, the range of communication could be increased to overcome foliage attenuation and other losses, thereby improving the communication range to that desired by the commanders.

Figure 1 shows an illustration of a typical deployment of troops using PRRs in an operation conducted in a highly dense deciduous tree environment and shows how collaborative beamforming can be applied. In a typical deployment, three dismounted soldiers form an operational unit. The soldiers usually operate close to one another with a separation distance no more than 5 meters for close combat support. Each operational unit can either communicate with their attached vehicle or with another operational unit. The communication range for a single PRR transmission in this environment is less than a hundred meters which is well below the few hundred meters achievable in line of sight conditions. With collaborative beamforming, the soldier PRRs will transmit an identical

message at the same time which combines coherently to overcome the effects of the foliage environment and extend the communication range to reach the intended recipient. Even in a benign environment, collective beamforming can extend the range of the system over what is achievable with a single user.

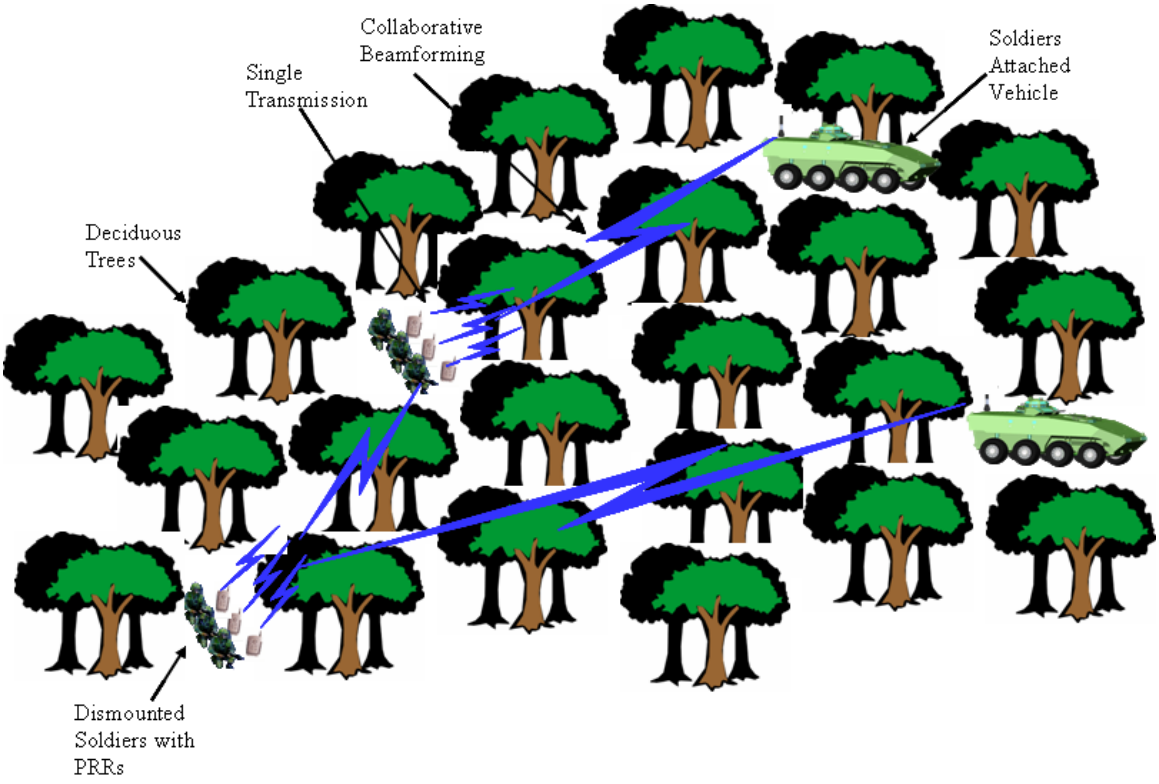

Figure 1. Typical deployment of troops using PRRs and illustration of collaborative beamforming.

In a traditional (centralized) multi-antenna transmitter, one way to perform beamforming is by exploiting reciprocity to estimate the complex channel gains to each antenna element. These channel gains are then computed in a centralized manner with reference to a RF carrier signal supplied by a local oscillator. This is not applicable in a distributed multi-antenna transmitter system used by the PRRs, where each soldier's PRR transmitter has separate RF carrier signals carried by separate local oscillator circuits. The challenge is to achieve synchronization in terms of carrier frequencies, carrier phases and symbol timing so that of all individual electromagnetic waves are coherent and add constructively when received by the antenna at the base station [2].

Wireless beamforming strategies for the PRRs need to be devised, and an analysis on system performance, tradeoffs and capabilities needs to be performed. System synchronization of the wireless collaborative communication network needs to be looked at in detail, as it is a major challenge due to the lack of fixed infrastructure and the dynamic topology of the PRR network. Jamming effects on PRR performance during operations need to be understood. These studies will help to meet the commanders requirements and aid the deployment of PRR systems out in the field during mission operation. These analyses will contribute in the development of the following research.

1. Distributed Beamforming Performance on PRR System

Different permutations of PRRs and distances away from each other give different performance results in terms of communication range. By devising different scenarios according to mission operations profile, the performance of a wireless beamforming application can be evaluated. Future mission profiles can be further enhanced based on the results. Various beamforming algorithms have been evaluated.

2. Seasonal Foliage Effects on Distributed Beamforming Performance

PRRs operating in different types of foliage density and seasonal environment generate different results in terms of communication range. These results will enable commanders to make well informed decisions on the limitation of PRR systems operating in different environments.

3. Synchronization of Wireless Distributed PRR System

In order to implement distributed beamforming effectively, synchronization between PRRs must be achieved to ensure that voice and data are transmitted correctly. Different synchronization schemes for the PRR system are presented which will contribute to the realization of implementing distributed beamforming of the PRR system.

C. THESIS OBJECTIVE

Communication is a treasured commodity in the battlefield. Restricted communication due to environmental factors has limited system performance short of the full potential of the system capabilities. One example is the significant degradation in communication range of the PRR system operating in a foliage environment. Such factors can be overcome by technological advancement and research. The goal of this thesis is to study and lay the framework to improve the communication constraints of a particular PRR system employing distributed beamforming and examine the challenges of implementing such strategies. A scenario of three soldiers with PRRs operating as a network with a static receiver vehicle as base station is simulated for various physical arrangements between PRRs and vehicle. Likewise, a scenario of two operational units operating as a network is simulated for various physical distances between the two units. The performance and limitations of beamforming at this stage is captured and analyzed. The captured data is then used in the foliage and seasonal simulated environment to determine its effects on beamforming and its feasibility. A synchronization scheme to ensure effective beamforming is evaluated, with its advantages and disadvantages presented.

The distributed beamforming performances are analyzed based on:

- Received power at the static vehicle receiver antenna.
- Improvement in gain and signal to noise ratio.
- Distance between the soldier PRRs and base station or soldier PRR to achieve sustainable communication.
- Array factor.

The environment and seasonal effects of foliage are analyzed based on

- Density of the tree leaves.
- Seasonal variation (winter and summer).

The synchronization schemes for distributed beamforming are analyzed based on

- Mutual synchronization.
- Master and slave synchronization.

These results will assist the commanders in the understanding of the PRR system performance under various conditions.

D. PREVIOUS WORK

The realization of a distributed beamforming network has several technological challenges. One is phase and time synchronization. Another is the rapid transfer of data between the PRRs and the digital beamformer, and data processing speeds fast enough to permit real-time operation. In a dynamic environment where the PRRs are distributed depending on the whereabouts of the soldiers, the position of the PRRs must be known to within a fraction of a wavelength in order to compensate for phase errors and dispersion [3].

The concept of a distributed beamforming network is not new. Long baseline interferometry is used in astronomy and employs many of the same principles as wireless beamforming [4]. Lee and Dorny [5] proposed a very large array using data collection from a fleet of ships, and proposed a "self-survey" technique to calibrate the system. Galati and Losquadro [6] described an air surveillance radar system where a constellation of satellites forms the radar array. Coherence and position location are achieved by optical measurements, and a communication system sends the elementary data to a master satellite for processing. Distributed array radar and its noise limited detection characteristics is described in [7].

Ochiai, Mitran, Poor and Tarokh [8] have analyzed the performance of collaborative beamforming in wireless ad hoc sensor networks using the theory of random arrays. The study shows that given a number of nodes randomly distributed over a large disk, a nice beam pattern can be formed with narrow mainlobe and average sidelobes as low as $1/N$, where N is the number of elements. The analysis is based on the ideal assumptions that the nodes and channel are static over the communication period and that the information rate is assumed to be sufficiently low that inter-symbol interference (ISI) is considered negligible.

Barriac, Mudumbai and Madhow [9] have studied the distributed beamforming approach for energy efficient transfer of data from sensors in sensor networks. The

studies show how placement errors, which translate to phase errors, affect the gains achieved by distributed transmit beamforming. The finding is that as long as the distribution of placement errors is contained, large gains can still be realized using distributed beamforming. The crucial assumption is that phase synchronization errors between the master and slaves are small compared to the carrier wavelength so that timing errors can be neglected. In their latter study [10], synchronization in a distributed fashion by master and slave architecture is proposed where one node in the cluster serves as master and the rest of the sensor nodes are slaves. The study assumes fixed sensor placement. The finding is that as long as errors in range measurements or placement of the sensor nodes is within a fraction of a carrier wavelength, the proposed distributed beamforming strategies will achieve most of the gains available from a centralized beamformer.

E. THESIS ORGANIZATION

Chapter I has presented the motivation and objective of the thesis, and surveyed prior work done. Chapter II presents the operation characteristics of the PRR system and its technical specifications. Chapter III provides an overview on the theory of antenna beamforming. Antenna theory on a single transmitter and receiver antenna configuration is first presented. Using multiple transmitters for beamforming allowing higher gain and distance is shown. Various operating scenarios are simulated and their beamforming performances analyzed.

Chapter IV focuses mainly on foliage and its seasonal effects on the beamforming performance. Various operating scenarios in terrain with foliage are simulated and beamforming performances analyzed. Chapter V specifically focuses on synchronization challenges for beamforming. The chapter proposes and analyzes different synchronization schemes and the applicability in our work. An analysis of phase errors, which affect the gains achieved by distributed beamforming, are performed. Chapter VI provides the conclusions of the thesis. Recommendations are made and future work is proposed.

THIS PAGE INTENTIONALLY LEFT BLANK

II. PERSONAL ROLE RADIO SYSTEM

This chapter begins by exploring the various PRR systems employed by different military forces. Various applications are cited to give an overview of the application of this emerging technology. Next, the functional blocks and components of a specific PRR system are described. The technical specification of a PRR system is presented. Following which, various trial scenarios and performance of the system are presented. The discussion on the constraints and limitations of deploying the PRR system in the field trial concludes this chapter.

A. INTRODUCTION TO PERSONAL ROLE RADIO SYSTEM

The PRR system forms an integral part of the sensor to shooter loop in the Ground Forces Networked Centric System paradigm shown in Figure 2, envisaged for information warfare. The wireless communication system provides connectivity in terms of data and voice between the soldiers ("Troops to Troops") and between the soldiers and their vehicle ("Vehicle to Troops"), and through the vehicle communication system to the higher echelon of commands. The soldiers on the ground play the role of mission execution and are paramount to any mission success.

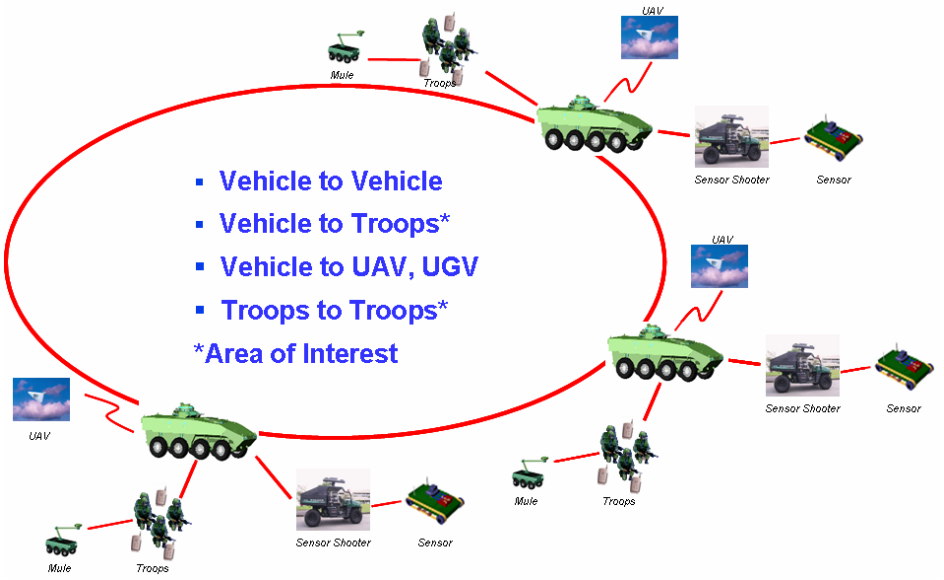

Figure 2. Ground forces network centric system.

A PRR is a short range radio operating independently of any infrastructures. PRRs offer effective communications within the mission operating squad and between combat teams, enabling cohesive dismounted infantry operations. The PRR can be operated hands-free allowing greater freedom of mobility to the soldiers. Present PRR systems are functioning in the 2.4 GHz and upper UHF bands, offering effective short range communications with low interference and adequate bandwidth utilization. Most systems operate in duplex conference operating modes, where the commander can speak to all his soldiers and get their responses, or in selective peer to peer communications, which is one to one. PRR systems support mainly voice but some can also transfer data at low bit rate. The PRR system replaces the heavier and cumbersome UHF/VHF radio man-pack, transforming a traditional soldier into a lighter, faster and more mobile future fighting force readily plugged into the main grid of the digital battlefield.

Table 1 shows the various PRR equivalent systems in the developing stages by military forces around the world. It can be seen clearly that the PRR system is one of the major development thrusts towards the vision of Future Combat System or equivalent initiatives by modern army forces.

Table 1. PRR type systems

Type	Frequency (GHz)	Power	Range	Manufacturer	Country
Future Infantry Soldier Technology (F.I.S.T.) : CWICS 200	2.4-2.4835	0.1-100mW	800m (LOS)	Cobham Defence Communications	United Kingdom
PNR 500	0.41 - 0.45	N.A.	800m (LOS)	Tadiran Communications Ltd.	Israel
Future Combat System (FCS): Soldier Radio Waveform	Band 1 & 2: 0.45 - 1 Band 3: 0.35 - 2.7	N.A.	N.A.	General Dynamics Decision Systems	United States
Felin (Soldier Personal Digital Radio)	DECT: 1.88-1.9 in Europe, 1.92-1.93 in U.S.	N.A.	N.A.	Sagem Defense Securite	France

1. Application

A PRR system interfaces the voice and data communication aspects of the Future Soldier equipping. The system acts as a gateway for information transfer between the soldiers and their attached vehicle. Other than the PRR system, future soldiers are

typically equipped with a portable computer for data processing, health monitoring system, advanced handheld computing capability functions such as mapping, navigation and freehand sketching of pre-determined tactical symbols. A PRR system provides linkage for the "Observation" and "Action" cycle of the OODA (Observation, Orientation, Decision and Action) loop [11]. Without the PRR system communication link, the future soldier will lose networking capability, almost immediately rendering the rest of the soldier's technological insertion useless. From a mission prospective, the mission success may be affected.

a. Voice Communication

A PRR system provides wireless voice communications between the soldiers and their attached vehicle. Soldiers on the ground rely on their PRRs to maintain communication links for instructions from commanders and reporting observations on the ground for commander decision making. Most PRR systems operate in duplex conference operating modes, where the commander can communicate with all his soldiers simultaneously or operate in selective peer-to-peer modes allowing dedicated communication between two users. Digital speech encoding provides high quality speech between the users.

b. Data Communication

A PRR system also provides wireless data communications between the soldiers and their attached vehicle. Soldiers on the ground can perform data transfer of information collected using the PRR communication links to their attached vehicle and vice versa. Similarly, commanders can send encrypted data to their soldiers to carry out orders. The PRR system acts as a gateway for the rest of soldier data processing equipment to transmit and receive data.

c. Geolocation

Soldiers in a dire situation can be geolocated from the PRR broadcast. If a soldier is in distress, the health monitoring system will activate an alarm signal. Since the soldier health monitoring system is hooked up to the PRR system, the alarm signal is

broadcast through the PRR system allowing the position of the distressed soldier to be located. A medical or support team can be dispatched to assist the soldier.

2. Performance Metrics for Personal Role System

A list of metrics is proposed to access the performance of a PRR system.

a. Energy Efficiency

Since PRRs are designed to be deployed in the field, they are normally powered by batteries with limited usage in hours. With efficient energy usage, the energy resource can be maximized and the lifetime of the network will be extended.

b. Maximum Communication Range

With limited power, the communication range between PRR and its receiver base station, and between PRRs within a unit are limited to a few hundred meters with clear line-of-sight (LOS) conditions.

c. Number of Communication Channels

The number of communication channels determines the number of users in the network.

d. Scalability

The PRR system allows the insertion and extraction of soldiers into or out of the network without affecting performance as long as it is within the allowable number of channels.

B. ROVIS/ANVIC-3 AND CWICS 200 SYSTEM

The Cobham Wireless Integrated Communications System (CWICS) 200 system is the specific PRR system chosen for study in this thesis. The CWICS 200 system provides a cordless extension to the ROVIS/ANVIC-3 family of products from Cobham Defence Communications Limited (CDC) for dismounted soldiers. The ROVIS AN/VIC-3 vehicle intercom (VIC) systems have been installed on military platforms such as: Abrams, Bradley, BCT (brigade combat team) Stryker in the U.S. Army, and Bronco and

Bionix in the Singapore Armed Forces. Figure 3 shows a generic block diagram of the ROVIS AN/VIC-3 system with CWICS 200 system. [12]

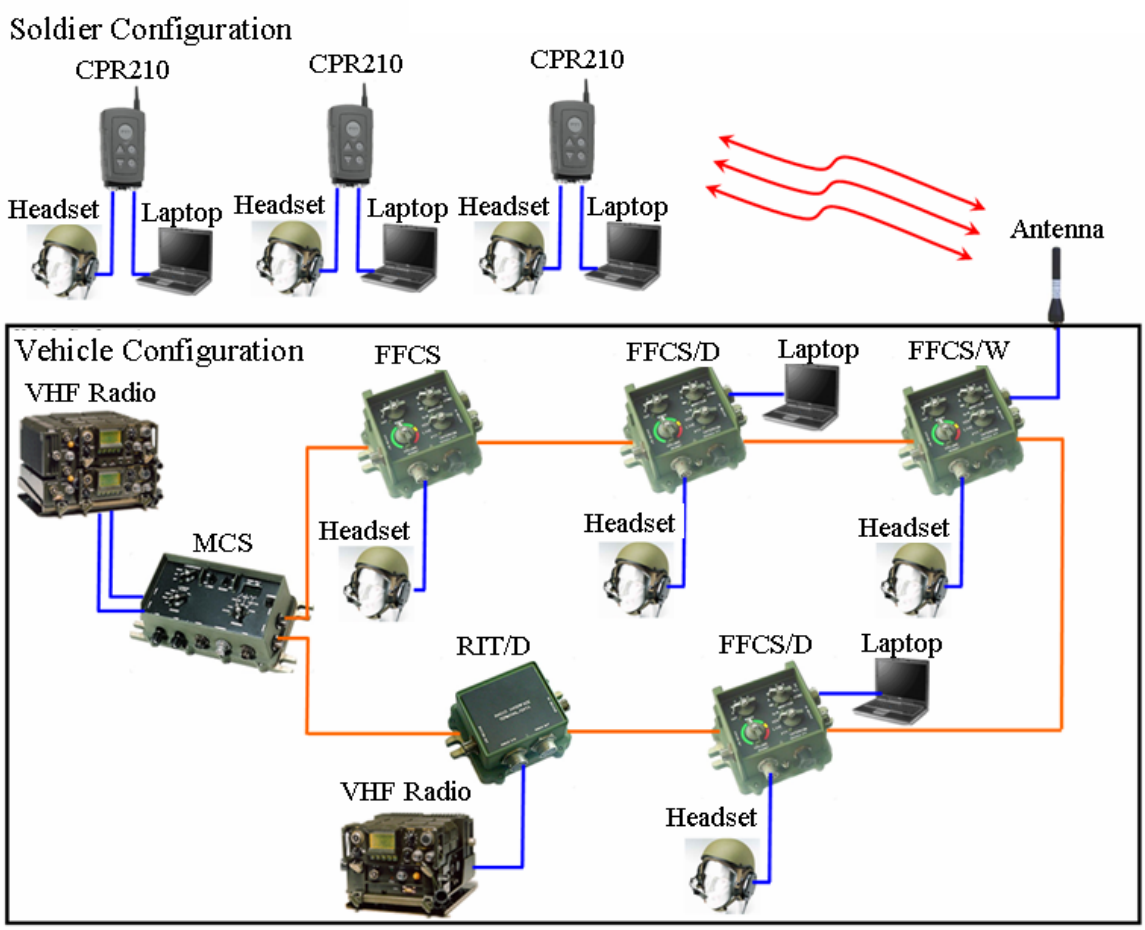

Figure 3. ROVIS AN/VIC-3 system. (After [12])

1. System Components

The ROVIS AN/VIC-3 system shown in Figure 3 comprises of the following hardware components. [7]

a. Master Control Station

The ROVIS Master Control Station (MCS) controls all intercom audio distribution and interfaces directly with vehicle alarms, two radio transceivers, an external field telephone or another vehicle intercom system. The MCS interfaces directly

with vehicle prime power and provides a regulated DC power supply to the rest of the system, including an independent regulated DC power supply to support up to ten Active Noise Reduction (ANR) headsets. The MCS controls the communications between up to six FFCS stations (or variants), a loudspeaker and up to six on-board radio transceivers (HF, UHF or VHF types).

b. Full-Functional Crew Station

The Full Function Crew Stations (FFCS) provide operators with all communication capabilities, limited only by MCS control. Controls on the FFCS permit its operator to talk and listen on the intercom, to transmit and receive from any one of six possible radios, or to transmit on one of the six possible radios whilst monitoring any one (or all) of the others. The crew station operator is able to choose between push-to-talk (PTT), continuous (live), and voice activated mic keying (VOX) of the intercom. The VOX of each FFCS independently tracks the ambient vehicle noise level and has an automatically adjustable threshold, so as to preclude inadvertent (unintentional) keying of the intercom. The VOX is not capable of keying any radio.

There are different types of FFCS variants:

(1) Full-Functional Crew Station/Data. The Full Function Crew Station with Data (FFCS/D) interface provides operators with all the communication capabilities of the standard FFCS described in Section II.B.1.b. It provides an additional industry-standard asynchronous RS232C interface to Data Terminal Equipment. The FFCS/D supports full-duplex high-speed digital data transfer at up to 57.6 kbps. Data transfer is supported between two FFCS/D stations or between a FFCS/D station and data-capable radios connected via RIT/Ds, or between CWICS 200 and a FFCS/D station via the FFCS/W. During data transfer, the FFCS/D retains full receive and transmit voice capability.

(2) Full-Functional Crew Station/Wireless. The Full Function Crew Station with Wireless (FFCS/W) interface provides dismounted soldier operation while retaining operators with all the communication capabilities of the standard FFCS described in Sections II.B.1.b. The FFCS/W routes all of the internal communication

paths to the external CPR210 (PRR) carried by the dismounted soldier over the 2.4 GHz wireless link. Dismounted soldiers can access this information and control up to three of the on-vehicle radios using the integrated PTT switches on the PRR.

(3) Remote Interface Terminal/Data. The Radio Interface Terminal with Data Interface (RIT/D) enables the connection of two data-capable radio transceivers using the industry-standard asynchronous RS232C data interface to an existing ROVIS system, up to the system maximum of six radios (using two RIT/D stations). The RIT/D supports full-duplex high-speed data transfer at up to 57.6 kbps between a FFCS/D station and connected radios. It also supports simultaneous analog voice signals to/from the same radio. The RIT/D has no user-adjustable controls.

(4) CWICS 200 System. The CWICS 200 system comprises of FFCS/W and the CPR210 PRR. It operates as a full duplex wireless intercommunication for six dismounted soldiers simultaneously, with the ability to listen and access remotely up to two on-vehicle radios connected to the ROVIS system. The access point for the CWICS is the FFCS/W over the 2.4 GHz wireless link. The FFCS/W is connected to a 7 dBi antenna that is mounted on the roof of the vehicle, whereas the PRR is equipped with a 3 dBi antenna for wireless transmission and reception function. Table 2 shows the technical specifications of a CWICS 200 system.

Table 2. CWICS 200 system technical specifications. (From [12])

Parameters	**Technical Specifications**
Number of channels	50 user selectable channels
Number of users	30 units in each conference group (1 master + 29 slaves)
Number of speakers	Up to 6 simultaneous speakers (1 master + 5 slaves)
Frequency	2.4 – 2.4835 GHz ISM band, frequency hopping TDMA using 20 frequencies per user channel
Transmit power	0.1 – 100 mW
Base Station power	1 W
Transmit Antenna Gain	3 dBi
Base Station Antenna Gain	7 dBi
Range	Up to 800 m (line-of-sight)
Operating time	16 hours
Size	28 x 73 x 128 mm
Weight	300 g including battery

C. PRR SYSTEM FIELD TRIAL

A field trial [1] was conducted in Singapore from 13th to 16th June 2005 for the commander to evaluate the performance of the ROVIS ANVIC/3 system and CWICS 200 system based on different operating scenarios. The objective of the field trial was to carry out a subjective user-evaluation of :

(i) ROVIS ANVIC/3 and CWICS 200 system performance,

(ii) On-board VHF radio performance, and

(iii) Data-transfer performance to and from dismounted soldiers.

1. Field Trial Equipment Setup

A FFCS/WS and three PRR (CPR-210) handheld radios were installed on two ROVIS-equipped Bronco vehicles to create a Full-Duplex Wireless Intercom Extension to each for dismounted soldier operation. The PRR system was integrated with an in-service VHF radio installed in each of the vehicles to test both the voice and data capability.

2. Conditions of Test

Various field operational scenarios were created for the commander to understand the capabilities and limitations of the PRR system. Wireless range tests were performed in two scenarios: (i) Open flat test area of at least 1 km radius around the vehicle, and (ii) Second area 5 kilometers distant from the first, but with good VHF in order to test voice/data rebroadcast of CPR-210 via the VHF net.

a. PRR Range Test

The soldier PRRs were connected to Bronco #0 (operating on Channel 0). The commander and the contractor representative went out onto the test track in a Land Rover with Bronco #0 left behind in the compound. Communications were maintained with Bronco #0 for aPRRoximately 300 meters before moving behind a high feature, losing both line-of-sight and communication.

b. Urban Warfare Scenario

An urban warfare scenario was simulated using Bronco #1 on the parade square from which soldiers were deployed with PRRs (CPR-210). The troops were deployed around the square and into a four level concrete building. All communications appeared to function satisfactorily throughout the building – including from inside the elevator. The communication range between the vehicle and the PRRs was about 400 m. Throughout the test, Bronco #1 was the master, and was used both stationary and whilst driving around the parade square. VHF rebroadcast was also demonstrated using the CPR-210s attached to Bronco #1 to transmit over the on-board VHF radio to a remote operator of the CNR900 in Bronco #0 which was located about 800 meters away in another compound.

c. Foliage Scenario with Autonomous Group

The CPR-210 PRR was tested while operating as an autonomous group (apart from any vehicle). The commander and one of his soldiers together with the contractor representative walked into a foliage environment. The three of them slowly moved apart to test the PRR range in the woods with dense tall deciduous trees until communication was lost. The communication range was found to be approximately seventy meters.

3. Field Trial Results

Table 3 summarizes the field trial results for the PRR system operating in various scenarios.

Table 3. PRR system field trial results. (After [1])

Operating Scenario	PRR Range Performance (meters)	Comments
Line of Sight	800	Manufacturer Specification
Range Test	300	Communication loss due to a high feature
Urban Warfare	400	No loss of communication inside the elevator
Foliage	70	Communication loss within a short distance due to environment

D. PRR SYSTEM PERFORMANCE

Comparing the manufacturer specifications of the PRR system in Table 2 and the field trial results in Table 3, it can be seen that the PRR range performance degrades significantly in the non-line of sight environment (from 800 meters in the specifications to 70 meters in the foliage environment during the field trial). This reduction in range performance affects mission operation profile and limits the full potential of employing such systems. While equipping the soldiers with PRRs are essential to fulfill the role of Future Soldier, the degradation aspects of the environment to the system cannot be ignored and need to be overcome.

E. SUMMARY

This chapter presents the various PRR systems employed by different military forces. Various sample applications were given to provide an overview of the application of this emerging technology. The functional blocks and components of a specific PRR system were described and the technical specification of a specific PRR system (CWICS 200) was presented. Results of field trials of various scenarios and corresponding performance of the system reported in [1] were summarized. The discussion on the constraints and limitations of deploying the PRR system in the field trial concluded this chapter.

The next chapter presents the concepts of distributed beamforming. The chapter includes analysis and discussion of Matlab simulated results based on various operational scenarios using collective beamforming techniques.

III. DISTRIBUTED BEAMFORMING

This chapter begins by presenting some concepts in electromagnetics that are relevant to distributed beamforming. Next, the rationale and simulation model for the distributed beamforming is described. Following which, the results of the simulation are presented. Finally, the discussion of the simulated results concludes this chapter.

A. ANTENNA FUNDAMENTALS

A transmitting antenna converts a time-varying alternating current (or voltage) that is encoded with data or a message at its input into propagating electromagnetic waves. On the other end, a receiving antenna converts the incident electromagnetic waves back to voltage or current from which the data or message is recovered. Successful communication in most narrowband systems requires that some of the energy that originates at the transmit antenna arrives at the receiver's antenna are smaller-amplitude replicas of those transmitted. [13, 14]

1. Antenna Radiation Pattern

An electromagnetic field propagates at the speed of light c in free space. A fundamental equation is:

$$\lambda = \frac{c}{f} \tag{3-1}$$

where $c = 3 \times 10^8$ m/s, f is the frequency in Hz and λ is the wavelength in meters.

The radiation pattern of an antenna displays the angular variation of radiated or received power as a function of direction in space at a fixed far field distance from the antenna. By fixing the antenna at the origin of a coordinate system, the vehicle antenna in our case, the radiation pattern can be derived by measuring the power density at all points on the surface of a sphere at a distance r from the vehicle antenna. The spherical coordinate system, shown in Figure 4, is used to describe the radiation pattern. The PRRs are assumed to be distributed over the x-y plane. There are N PRRs deployed over a local area depicted by the circle in Figure 4. The nth node location is denoted in three

dimensional Cartesian coordinates (x_n, y_n, z_n). The location of the observer (another PRR or the vehicle, which is also referred to as the base station) is denoted in spherical coordinates (r, θ, φ) or by (x, y, z). The elevation angle is $(90^0 - \theta)$ which varies from 0^o to 90^o and the angle φ is the azimuth angle which varies from 0^o to 360^o. Once the distance r is fixed, the power density is a function of θ and φ. [3, 9]

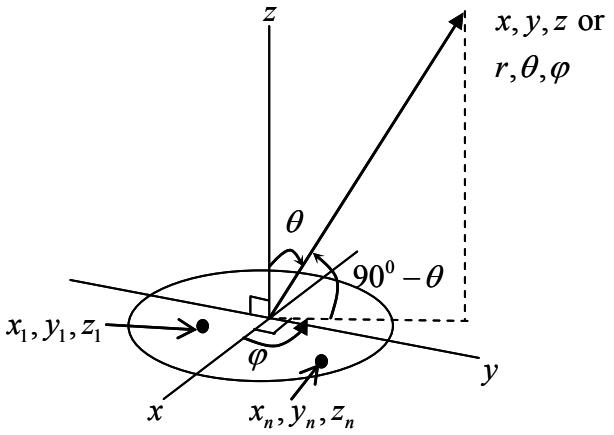

Figure 4. Spherical coordinate system notation. (After [3])

The PRR antennas are of isotropic type. An isotropic antenna radiates electromagnetic energy uniformly in all directions. Therefore, since power radiates uniformly, the same power density value appears at any point on a sphere centered at the origin. If the transmitting isotropic antenna is radiating a power of P_t in watts, then the received time-averaged power density W in $\mathrm{W/m^2}$ at any point on the sphere surface of radius r centered at the source is given by

$$W = \frac{P_t}{4\pi r^2} = \frac{\left|\bar{E}\right|^2}{2\eta_0} \tag{3-2}$$

where $4\pi r^2$ is the surface area of a sphere of radius r and $|E|$ is the electric field intensity (peak value). Therefore, in free space, the power density W is inversely proportional to the square of the distance of the transmitter. [3]

2. Directivity and Gain

The directivity of an antenna is defined as the ratio of the radiation intensity in a certain direction to the average radiation intensity and is given by the equation

$$D = \frac{4\pi}{\Omega_A} = \frac{1}{\frac{1}{4\pi}\iint_{4\pi}\left|\bar{E}_{norm}(\theta,\varphi)\right|^2 d\Omega} \tag{3-3}$$

where Ω_A is the antenna beam solid angle, and D is the directivity (dimensionless). Directivity does not account for any antenna loss. $\left|E_{norm}\right|$ is the normalized electric field intensity.

For an antenna with a single main lobe pointing in the z-direction as shown in Figure 5, Ω_A can be approximated as the product of the principal plane half power beamwidths φ_{HPBW} and θ_{HPBW} [13, 15]. Consequently,

$$D = \frac{4\pi}{\theta_{HPBW}\varphi_{HPBW}} \tag{3-4}$$

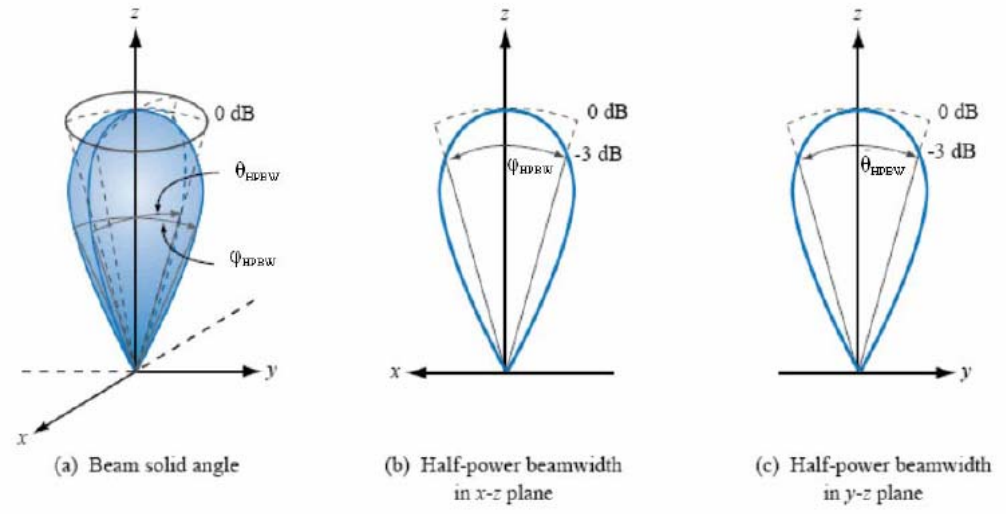

Figure 5. Antenna directivities. (From [13, 15])

The gain of an antenna, *G,* is defined relative to the power into the antenna and thus includes loss. In practice, the gain of an antenna can be determined from its effective area, A_e, and the wavelength, λ by [13]

$$G = \xi D = \frac{4\pi A_e}{\lambda^2} \tag{3-5}$$

where ξ is the radiation efficiency given by

$$\xi = \frac{P_{radiated}}{P_{input}} \quad (0 \le \xi \le 1) \tag{3-6}$$

3. Antenna Polarization

The energy radiated by any antenna is contained in a transverse electromagnetic wave that is comprised of electric and magnetic field vectors. These vectors are always orthogonal to one another and orthogonal to the direction of propagation for plane and spherical waves. For antenna polarization, the electric field vector of the electromagnetic wave is usually used to describe its polarization. In general, all polarizations are elliptic. The total electric field of the wave is comprised of two linear components, which are orthogonal to one another. Each of these components has a different magnitude and phase. At any fixed point along the direction of propagation, the tip of the total electric field vector would trace out an ellipse as a function of time. The two limiting cases of elliptical polarization are circular and linear. [13]

A circularly polarized electromagnetic wave is comprised of two linearly polarized electric field components that are orthogonal, both having equal amplitude but 90 degrees out of phase from each other. In this case, the polarization ellipse traced by the wave is a circle. Depending upon the direction of rotation of the electric field vector, the wave will be left-hand circularly polarized or right-hand circularly polarized. The phase relationship between the two orthogonal components, +90 degrees or –90 degrees, determines the direction of rotation. [13]

A linearly polarized electromagnetic wave is comprised of a single electric field component, and the polarization ellipse is a straight line. Most wireless systems are designed to operate with linear polarization, usually vertical with respect to the ground. [14]

4. Free Space Link Equation

Consider a free-space communication link between two antennas, with separation distance r being large enough for each antenna to be in the far-field region of the other. The transmitting and receiving antennas have effective areas A_t and A_r, respectively. Both the antenna gains can be related to their effective areas by Equation (3-5). If the transmitting antenna at the origin with gain G_t radiates P_t watts and the receiving antenna has gain G_r, the received power at a distance r is given by [3, 13]

$$P_r = \frac{P_t G_r G_t \lambda^2}{(4\pi r)^2} \tag{3-7}$$

5. Antenna Far Field Conditions

In the near field of an antenna, the fields exhibit spherical wave behavior and have $1/r$ magnitude dependence, where r is the distance from the antenna. In the far-field region, the radiation pattern is independent of distance. The conditions for determining the minimum distance from an antenna for far-field behavior are given in the following equations [16]. The first is

$$r \geq r_{ff} = \frac{2L^2}{\lambda} \tag{3-8}$$

where L is the largest dimension of the antenna. The far-field region is all ranges $r \geq r_{ff}$ and r_{ff} is called the far-field distance. A second requirement is that

$$r \gg L \tag{3-9}$$

That is, the far field r is very large compared to the antenna size, Finally the third requirement is

$$r \gg \lambda \tag{3-10}$$

Equation (3-10) follows from $kr = 2\pi r/\lambda \gg 1$, where $k = 2\pi/\lambda$. Table 4 summarizes the field region distances for cases where $L \gg \lambda$.

Table 4. Far field distance. (After [16])

Region	**Distance from antenna (*r*)**
Reactive near field	0 to $0.62\sqrt{L^3/\lambda}$
Radiating near field (Fresnel Region)	$0.62\sqrt{L^3/\lambda}$ to $2L^2/\lambda$
Far field (Fraunhofer region)	$2L^2/\lambda$ to ∞

In most cases the limiting distance for any finite antenna of dimension L is $2L^2/\lambda$. This zone is called the Fraunhofer region if the antenna is focused at infinity (the rays at large distances from the antenna when transmitting are parallel). In the far-field region, the radiation pattern is independent of distance. The zone interior to r_{ff}, called the near field, is divided into two sub regions. The reactive near-field region is closest to the antenna and is the region for which the reactive field dominates over the radiative fields. This region extends to a distance of $0.62\sqrt{L^3/\lambda}$ from the antenna, as long as $L \gg \lambda$. Between the reactive near-field and far-field regions is the radiating near-field region in which the radiation fields dominate and where the angular field distribution depends on distance from the antenna. For an antenna focused at infinity, the region is referred to as the Fresnel region. [16]

The far field region for the electrically small PRR antenna is very near to the antenna. For example, at 2.45 GHz ($\lambda = 0.122$ m) if a monopole and its image are $\lambda/2$ long then $r_{ff} \geq 2(0.0625)^2/0.122 = 0.064$ m. However, if two PRRs form a beam coherently, they comprise an array of length *L*, where *L* is their separation. For example, if the PRRs are 10 m apart then $r_{ff} \geq 2(10)^2/0.122 = 1639$ m. In this case, when the PRRs

employ collective beamforming the far-field condition will not be met and using the plane wave phase shifts to scan the beam (i.e., focusing at infinity) may not give the highest gain when the observation point is closer than 1639 m.

B. LINK EQUATIONS

Beamforming is the use of multiple individual antennas for transmitting or receiving the same electromagnetic wave in a coherent manner. The waves can be made to combine constructively, if the waves are perfectly coherent in terms of carrier phases, carrier frequencies and symbol timings. In this section the link equations (Friis equations) for simultaneous transmitters and receivers are derived.

1. Distributed Elements

Figure 6 shows the geometry of the general problem. In order to simplify the analysis, the following assumptions are made [3]:

- The location of each PRR is fixed.
- For our study, each PRR is equipped with a single ideal omnidirectional antenna.
- The PRR antennas transmit at equal powers.
- Base station (vehicle) antenna is high gain (7 dBi) omnidirectional.
- Mutual coupling effects among the PRR antennas are negligible.
- The base station (vehicle) is static (not moving) and the PRRs have knowledge of its exact location.

To begin with PRRs are assumed to be perfectly synchronized. Thus there is no frequency offset or phase jitter. A time-harmonic waveform is assumed with an $e^{j\omega t}$ time dependence ($\omega = 2\pi f$), so that phasors' quantities can be used.

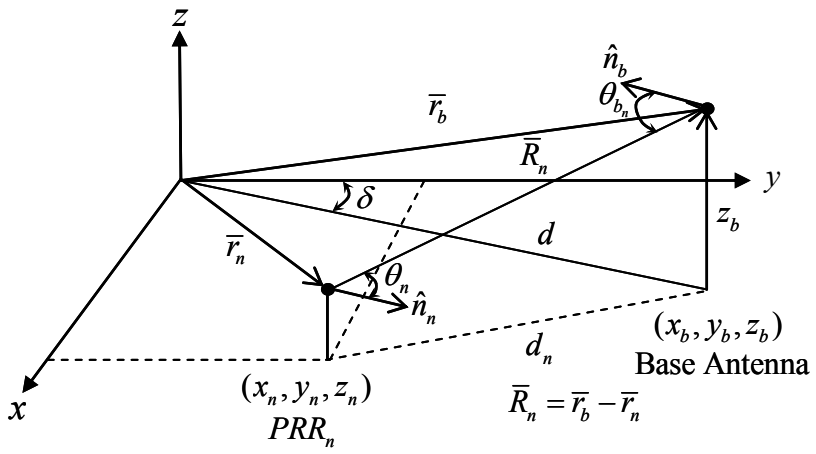

Figure 6. Distributed element notation. (From [17])

There are a total of N PRRs, where PRR_n has position vector $\bar{r}_n = x_n\hat{x} + y_n\hat{y} + z_n\hat{z}$. Hence forth, the remaining parameters are defined as [17]:

- P_{t_n} is the transmit power of PRR_n, assumed identical ($= P_{t_0}$).
- $G_n(\theta_n)$ is the gain of PRR_n antenna in direction of the base station.
- $G_b(\theta_n)$ is the gain of base station in direction of PRR_n.
- $\hat{n}_n$ gives the direction of maximum gain of the antenna for PRR_n. Usually the pattern of the PRRs are omnidirectional. Figure 7 shows an omnidirectional pattern, in which case $\hat{n}$ is irrelevant.
- The assumption is made that $d \gg z_n$ or z_b so that only the azimuth dependence in the antenna patterns is considered.
- δ is the angle from the line between the origin and base station. Patterns will be plotted as a function of this angle.

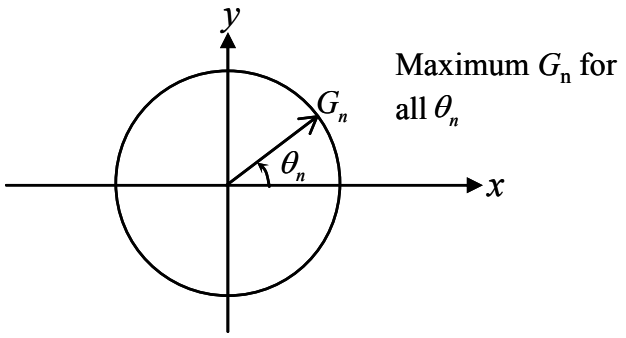

Figure 7. Omnidirectional azimuth pattern (top view) for $\hat{n}_n = \hat{x}$. (From [17])

a. Base Station Power Signal at PRR$_n$

For N distributed PRR elements, using the notation in Figure 6, the received signal at element n from the base station vehicle antenna is given by

$$P_{r_n} = \frac{P_{t_b} G_b(\theta_n)}{4\pi R_n^{\,2}} \frac{\lambda^2 G_n(\theta_n)}{4\pi} \left| F_n(\theta_n) \right|^2 \left(PLF_n \right)^2 \tag{3-11}$$

where $A_{e_n}(\theta_n) = \lambda^2 G_n(\theta_n)/4\pi$ is the effective area of PRR_n antenna in the direction of the base station, the PLF is the polarization loss factor for PRR_n antenna, $F_n(\theta_n)$ is a path gain factor between the base station and PRR_n.

If a single bounce multipath (flat earth model) signal is included, as illustrated in Figure 8, a simple expression for F_n results.

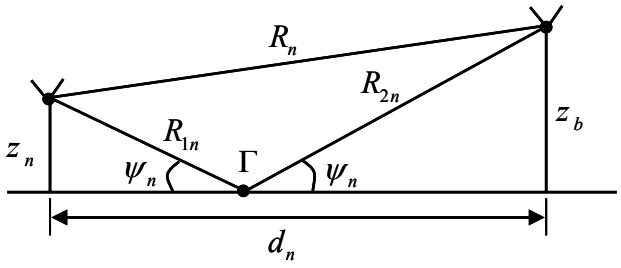

Figure 8. Single bounce multipath (flat earth model). (From [17])

Assume $d_n \gg z_n$ and z_b so that $d_n \approx R_n$ and the reflection coefficient of the surface is $\Gamma = |\Gamma| e^{j\theta_\Gamma}$. If the gains for the direct and reflected paths are equal

$$F_n = \frac{E_{d_n} + E_{r_n}}{E_{d_n}} = 1 + \Gamma e^{-jk\Delta R_n} \tag{3-12}$$

where $\Delta R_n = (R_{1n} + R_{2n}) - R_n \approx 2z_n z_b / d_n$. Including attenuation over the entire length of the paths:

$$F_n = e^{-\alpha_{d_n} R_n} + \Gamma e^{-\alpha_{r_n}(R_n + \Delta R_n)} \tag{3-13}$$

where α_{d_n} is the attenuation on the direct path and α_{r_n} is the attenuation on the reflected path.

For the simplest case where $\Gamma \approx -1$, which is true for small grazing angles, and $\alpha_{d_n} = \alpha_{r_n}$, the one-way voltage factor is given by

$$F_n \approx e^{-\alpha_{d_n}} \sin\left(\frac{kz_b z_n}{d_n}\right) \tag{3-14}$$

The electric field intensity incident at PRR_n is found from

$$\left|\overline{W}_{i_n}\right| = \frac{\left|\overline{E}_{i_n}\right|^2}{2\eta_0} = \frac{P_{t_b} G_b}{4\pi R_n^{\,2}} \left|F_n(\theta_n)\right|^2 \tag{3-15}$$

or,

$$\left|\overline{E}_{i_n}\right| = \sqrt{\frac{2\eta_0 P_{t_b} G_b}{4\pi R_n^{\,2}}} \left|F_n(\theta_n)\right| \tag{3-16}$$

where $\left|\overline{E}_{i_n}\right|$ is the peak electric field in V/m. The complex value is obtained by adding the phases. For the direct path only $|F_n(\theta_n)|$=1 and

$$\overline{E}_{i_n} = \left|\overline{E}_{i_n}\right| e^{-jkR_n} e^{j\Phi_b} \hat{e}_i \tag{3-17}$$

where Φ_b is the arbitrary phase of the transmitter and $\hat{e}_i$ is the direction of electric field vector (e.g., for vertical, $\hat{e}_i = \hat{z}$).

In order to form a receive beam collectively using *N* PRRs, the complex electric field samples from the individual antennas must be measured and sent to the central processor. Actually, complex voltages are measured at the antenna terminals that are linearly related to the incident electric fields at the antennas. The voltage can be obtained by either of two methods: Case 1: effective height or Case 2: effective area. Both cases can be represented in the form of an equivalent circuit shown in Figure 9.

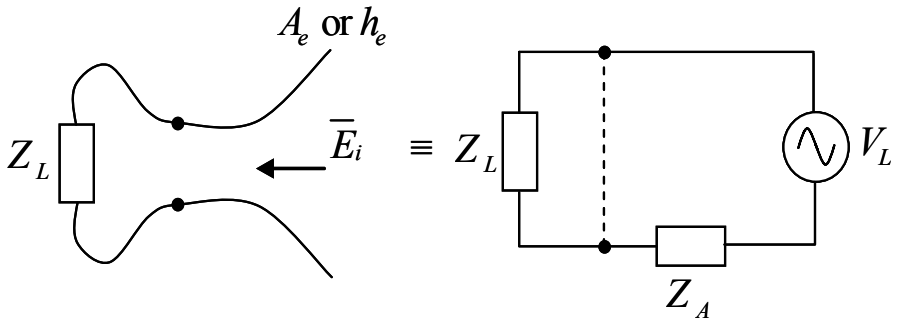

Figure 9. Equivalent Circuit. (From [17])

Case 1: Effective height

Voltage at the antenna terminal is given by

$$V_n = \overline{E}_{i_n} \bullet \overline{h}_e \tag{3-18}$$

where $\overline{h}_e$ is the effective height of the PRR antenna. This method gives the voltage directly.

Case 2: Effective area

From the incident power density (time averaged) the received power is

$$P_{r_n} = \left|W_{i_n}\right| A_{e_n} = \left|W_{i_n}\right| \frac{\lambda^2 G_n}{4\pi} \tag{3-19}$$

The power across the load R_L can be expressed by

$$P_{r_n} = \frac{1}{2}\mathrm{Re}\left\{V_L I_L^{\,*}\right\} = \frac{1}{2}\frac{\left|V_L\right|^2}{R_L} \tag{3-20}$$

Solving Equations (3-19) and (3-20) for the effective area gives

$$A_{e_n} = \frac{V_n^{\,2}}{P_{r_n}}\frac{R_L}{\left|Z_A + Z_L\right|^2} = \frac{V_n^{\,2}}{P_{r_n}}\frac{R_L}{(2R_A)^2} \tag{3-21}$$

when $Z_L = Z_A^{\,*}$ where $Z_L = R_L + jX_L$, $Z_A = R_A + jX_A$, and $R_A = R_l + R_r$ (R_l is the loss resistance and R_r is the radiation resistance). The effective height magnitude h_e and maximum effective aperture of PRR_n antenna are given by [18]

$$h_e = 2\sqrt{\frac{A_{e_n} R_r}{\eta_0}} \tag{3-22}$$

$$A_{e_n} = \frac{h_e^{\,2}\eta_0}{4R_r} \tag{3-23}$$

For the conjugate matched condition $R_A = R_L$ and $X_A = -X_L$,

$$V_n^{\,2} = \frac{P_{r_n} A_{e_n}\left(2R_A\right)^2}{R_L} = P_{r_n} A_{e_n}\left(4R_A\right)$$

Thus,

$$\frac{V_n^{\,2}}{4R_A} = P_{r_n} A_{e_n} \tag{3-24}$$

If there is no ohmic loss, then $R_A = R_r$ (all radiation resistance) and adding the phase shift gives the complex voltage for PRR_n

$$V_n = \sqrt{4P_{r_n} A_{e_n} R_r}\, e^{-jkR_n} e^{j\Phi_n} \tag{3-25}$$

Assuming a 50 Ω impedance and a $\lambda/4$ monopole ($D = 3.2$ or $A_e = \lambda^2 D/4\pi = 0.255\lambda^2$) gives

$$V_n = 0.87\sqrt{P_{r_n}}e^{-jkR_n}e^{j\Phi_n} \tag{3-26}$$

at 2.45 GHz. The important point is that V_n varies as a constant times $\sqrt{P_{r_n}}$. The constant depends on the particular antenna type, but does not enter into the beamforming calculation as all PRR antennas are identical and share the same constant. The complex voltages can be written as in phase and quadrature (I_n and Q_n) signals to be used later in digital beamforming

$$V_n = I_n + jQ_n \tag{3-27}$$

b. PRR$_n$ Signal at the Base Station

For *N* distributed PRR elements similar to the one PRR shown in Figure 6, the received signal at the vehicle base station antenna due to element *n* is given by

$$\begin{aligned} P_{b_n} &= \frac{P_{t_n} G_n(\theta_n)}{4\pi R_n^{\,2}} \frac{\lambda^2 G_b(\theta_{b_n})}{4\pi} \left|F_n(\theta_n)\right|^2 \\ &= \frac{P_{t_n} G_n(\theta_n) A_{e_b}(\theta_{b_n})}{4\pi R_n^{\,2}} \left|F_n(\theta_n)\right|^2 \end{aligned} \tag{3-28}$$

The propagation channel is assumed to be reciprocal, so this is the same F_n as shown in Equation (3-12). The electric field at the base station is determined from [17]

$$\left|\bar{W}_{i_n}\right| = \frac{P_{t_n} G_n(\theta_n)}{4\pi R_n^{\,2}} \left|F_n(\theta_n)\right|^2 = \frac{1}{2}\frac{\left|E_{b_n}\right|^2}{\eta_0} \tag{3-29}$$

The complex electric field vector

$$\bar{E}_{b_n} = \hat{e}_n \left|E_{b_n}\right| e^{-jkR_n} e^{j\Phi_n} = \sqrt{\frac{2\eta_0 P_{t_n} G_n(\theta_n)}{4\pi R_n^{\,2}}} e^{-jkR_n} e^{j\Phi_n} \hat{e}_n \left|F_n(\theta)\right| \tag{3-30}$$

where Φ_n includes all phases introduced on the PRR side (synchronization, channel, hardware) except path, and $\hat{e}_n$ gives the electric field direction, which is determined by the physical orientation of the PRR antenna.

c. Total Signal Strength at the Base Station due to all PRR$_n$

If the base station antenna polarization is defined by the vector $\hat{h}_b$, then the total field at the base station is

$$\begin{aligned} E_b &= \sum_{n=1}^{N} \overline{E}_{b_n} \bullet \hat{h}_b = \sum_{n=1}^{N} E_{b_n} \hat{e}_n \bullet \hat{h}_b \\ &= \sum_{n=1}^{N} \sqrt{\frac{2\eta_0 P_{t_n} G_n(\theta_n) \left|F_n(\theta)\right|^2}{4\pi R_n^{\,2}}} e^{-jkR_n} e^{j\Phi_n} \hat{e}_n \bullet \hat{h}_b \end{aligned} \tag{3-31}$$

The total received power at the base station P_{r_b} is given by

$$P_{r_b} = \frac{1}{2} \frac{\left|E_b\right|^2}{\eta_0} A_{e_b} \tag{3-32}$$

where $A_{e_b} = G_b \lambda^2 / 4\pi$. Therefore

$$P_{r_b} = \frac{G_b \lambda^2}{(2\eta_0) 4\pi} \left| \sum_{n=1}^{N} \sqrt{\frac{2\eta_0 P_{t_n} G_n(\theta_n) \left|F_n(\theta)\right|^2}{4\pi R_n^{\,2}}} e^{-jkR_n} e^{j\Phi_n} \hat{e}_n \bullet \hat{h}_b \right|^2 \tag{3-33}$$

Assuming the following conditions:

- line of sight only, $F_n = 1$,
- neglect amplitude differences in incident waves, $\left|\overline{R}_n\right| = \left|\overline{r}_b\right|$,
- PRR elements are all synchronized, calibrated, scanned and focused, $kR_n + \Phi_n$ is constant for all *n*,
- equal PRR gains and powers, $G_n = G_0$ and $P_{t_n} = P_{t_0}$, and

- all antennas are parallel $\hat{e}_n \bullet \hat{h}_b \approx 1$ and $|\overline{r}_n| \ll d$ (localized distribution of PRRs),

Equation (3-33) reduces to

$$\begin{aligned} P_{r_b} &= \frac{G_b \lambda^2}{4\pi} \left| \sum_{n=1}^{N} \sqrt{\frac{P_{t_0} G_0}{4\pi r_b^{\,2}}} \right|^2 = \frac{P_{t_0} G_0 \lambda^2}{\left(4\pi r_b\right)^2} \left| \sum_{n=1}^{N} (1) \right|^2 \\ &= \frac{\left(NP_{t_0}\right)\left(NG_0\right)\lambda^2 G_b}{\left(4\pi r_b\right)^2} \end{aligned} \tag{3-34}$$

where NP_{t_0} is the total array transmitted power and NG_0 can be viewed as the gain of the distributed array when coherently phased.

d. Array Factor

From Figure 4, in the far field, the array factor of distributed PRR elements can be expressed by

$$\begin{aligned} AF(\theta,\varphi) &= \sum_{n=1}^{N} W_n e^{jk(x_n u + y_n v + z_n w)} \\ &= \sum_{n=1}^{N} A_n e^{-jk(x_n u_s + y_n v_s + z_n w_s)} e^{jk(x_n u + y_n v + z_n w)} \end{aligned} \tag{3-35}$$

where the phases to scan the beam to (θ_s, φ_s) are $u_s = \sin\theta_s \cos\varphi_s$, $v_s = \sin\theta_s \sin\varphi_s$, $w_s = \cos\theta_s$, and $u = \sin\theta\cos\varphi$, $v = \sin\theta\sin\varphi$, and $w = \cos\theta$. If $\theta = \theta_s = \pi/2$, and all antennas are at the same height $z_n = z_b = 0$, Equation (3-35) becomes

$$AF(\varphi) = \sum_{n=1}^{N} A_n e^{-jk(x_n \cos\varphi_s + y_n \sin\varphi_s)} e^{jk(x_n \cos\varphi + y_n \sin\varphi)} \tag{3-36}$$

The normalized array factor can be found from

$$\left|AF_{norm}\right| = \left| \frac{AF(\varphi)}{\max(AF)} \right| \tag{3-37}$$

If all PRR antenna element patterns are identical, $EF_n(\varphi) \equiv EF(\varphi)$, then the total array pattern is

$$\left|E_{norm}\right| = \left|EF_{norm}(\varphi)\right|\left|AF_{norm}(\varphi)\right| \tag{3-38}$$

Note that the phases to scan the beam in Equation (3-35) are based on a plane wave front. Hence the beam is focused at infinity.

e. Directivity of Antenna Array

From Equation (3-3), the expression for the directivity of the antenna array is given by

$$D = \frac{4\pi}{\Omega_A} = \frac{4\pi}{\int_0^{2\pi}\int_0^{\pi}\left|E_{norm}\right|^2 \sin\theta d\theta d\varphi} \tag{3-39}$$

For an arbitrary arrangement of the elements the integrals must be evaluated numerically.

2. Beamforming Concepts and Methods

a. Distributed Beamforming

Distributed beamforming (also called collaborative or collective beamforming) is illustrated in Figures 10 and 11. When the PRRs are receiving, as shown in Figure 10, the complex voltages from Equation (3-25) are weighted by the beamformer according to Equation (3-35). Using the known PRR and vehicle locations, the weights $\{W_n\}$ can be applied to obtain a maximum by constructive interference.

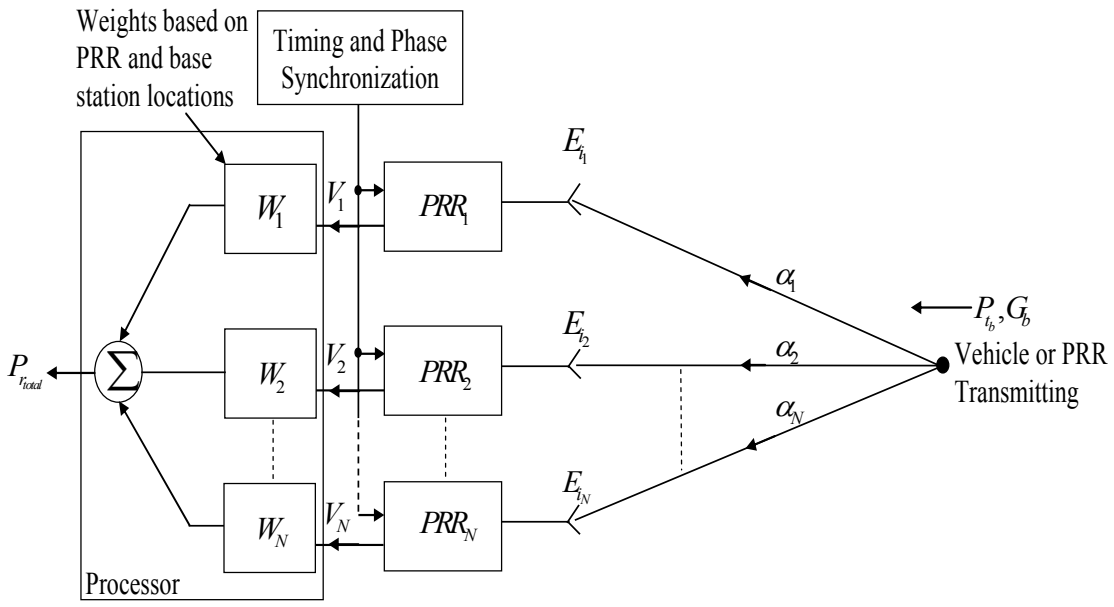

Figure 10. Collective beamforming on receive.

When the PRRs are transmitting, all radios transmit simultaneously as shown in Figure 11, with the proper time and phase delays so that all PRR signals arrive at the vehicle at the same instant and add constructively. In this case, the received power is given by Equation (3-33). With the stated assumptions, Equation (3-34) can be recast as

$$P_{r_b} = \left(N^2 P_{t_0}\right) \frac{G_0 \lambda^2 G_b}{\left(4\pi r_b\right)^2} \tag{3-40}$$

which indicates an increase in power by a factor of N^2 over a single PRR. [2]

b. Phase to Focus and Scan

There are two methods of forming a beam. The two methods are closed-loop beamforming and open-loop beamforming. For both cases, synchronization among PRRs is essential. [3]

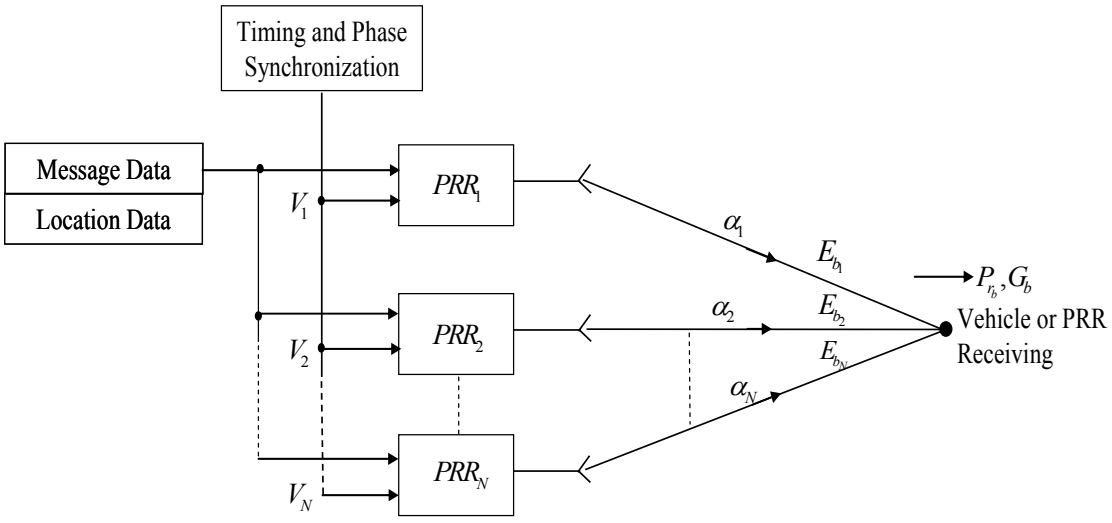

Figure 11. Collective beamforming on transmit.

Closed-loop beamforming requires a series of measurements between each PRR and the vehicle antenna. Therefore, this applies to the closed-loop case such as self-phasing arrays. [3]

Open-loop beamforming requires knowledge of the positions of all antennas relative to a common reference such as the vehicle antenna, and thus corresponds to the open-loop case [3]. Here it is assumed that all antenna positions are known to a fraction of a wavelength (≈0.01 m). The practical implications of this assumption are discussed later.

Because the base station can be in the near field of an array of PRRs, the proper phase shifts should be added to focus the collective beam at the base station. From Equation (3-33) the phase of PRR_n is $-kR_n + \Phi_n$. Using the local PRR coordinate system origin as a reference (Figure 6) a phase is inserted in PRR_n's signal so that

$$\begin{aligned} -kR_n + \Phi_n &= -kr_b \\ \Phi_n &= k(R_n - r_b) \end{aligned} \tag{3-41}$$

This phase will focus the beam at the base station, i.e., give a maximum in the electric field, assuming there are no other phase differences in the transmitter.

C. MATLAB SIMULATION

Matlab by Mathworks is the simulation and analysis tool used to study the antenna and propagation effects. Different PRR system configurations under field operating scenarios are modeled in Matlab. Two baseline models are used for reference: (1) a link between a single PRR and a vehicle antenna, and (2) a link between two PRRs. The results are used as a baseline for comparison with other scenarios. Analysis of the simulated results are presented and discussed. In these simulations, it is assumed that the positions of all antennas are known exactly and that all transmitters are perfectly synchronized.

1. Communication between Single PRR and Vehicle Base Station

The configuration of a single PRR and vehicle antenna base station is created as a reference model to understand the system performance and its limitations. Figure 12 shows the scenario configuration. This model is created with a clear path between the PRR and vehicle antenna unobstructed (line of sight) with no multipath fading or environmental losses. Two distances of separation are chosen, where d_1=400 m and 800 m, respectively. The rationale of choosing 400 m as a separation distance is that it was the maximum achievable distance during the field trial before communication was lost behind a large feature. On the other hand, 800 m was defined as the maximum achievable distance for line of sight in the PRR system specifications. These results will be used to compare with other configurations to evaluate performance improvement or degradation. [1]

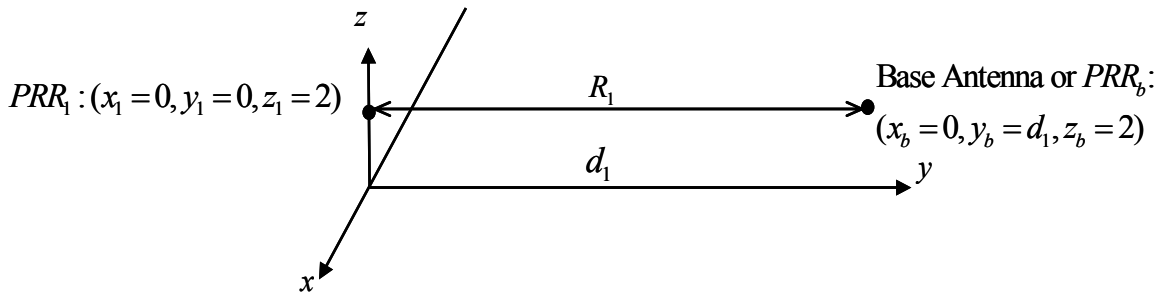

Figure 12. Single PRR configuration with PRR_1 at ($x_1 = 0, y_1 = q, z_1 = 2$) and base station at ($x_b = 0, y_b = d_1, z_b = 2$) in meters.

Figure 13 shows the plot of received power P_r at the vehicle base station versus distance. When the PRR antenna is at distances of d_1=400 and 800 m from the vehicle antenna, received powers P_r at the vehicle base station are –94.27 dBW and –100.29 dBW, respectively.

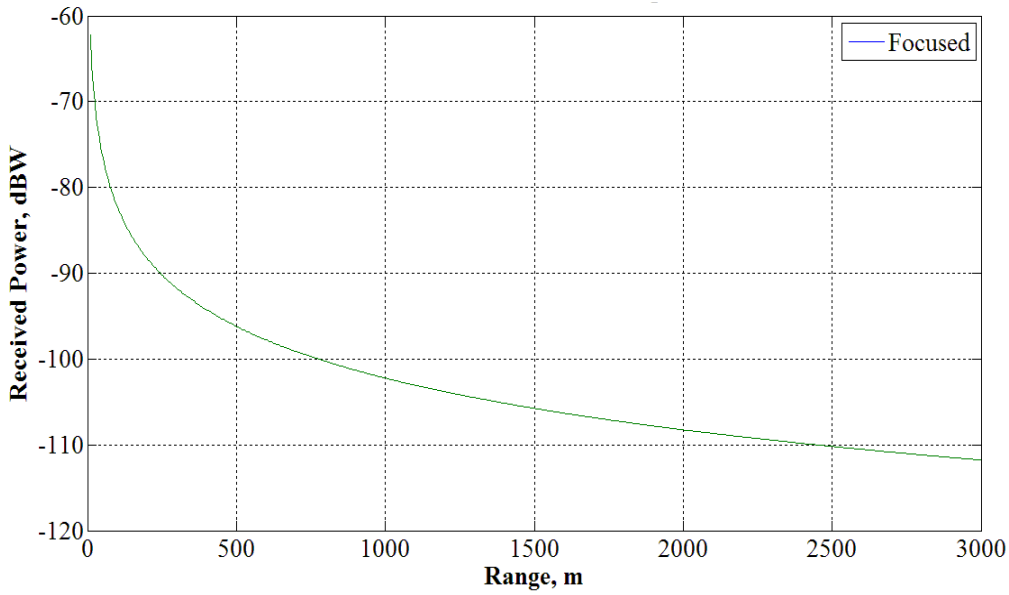

Figure 13. Plot of power signal received at base station for a single transmitting PRR.

Figure 14 shows the received power at the range of the PRR at 800 m. From the plot it can be seen that all the values are constant which means that any point on the plot is equal to –100.29 dBW from Figure 13.

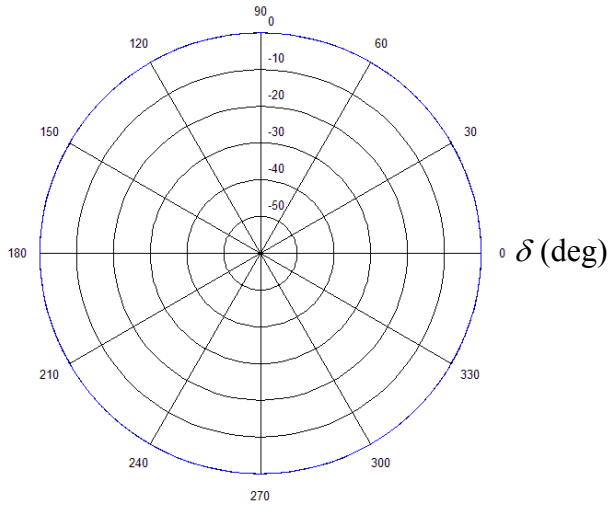

Figure 14. Normalized plot of received power at range of base station for a single transmitting PRR with d_1=800 m.

2. Communication between Two Single PRRs

The configuration of two single PRRs communicating is created based on field trial range test scenario in Table 3. During the field trial, communication between two single PRRs was effective for up to 300 m under a clear line of sight condition. Figure 12 shows the scenario configuration. The results will be used as a baseline to compare with other PRR configuration scenarios to evaluate performance improvement or degradation.

Figure 15 shows the plot of received power P_r at the receiving PRR versus distance. When the PRR antenna is at distances of d_1=400 and 800 m, the received powers P_r at the second receiving PRR in another operating unit are –100.26 dBW and –106.28 dBW, respectively.

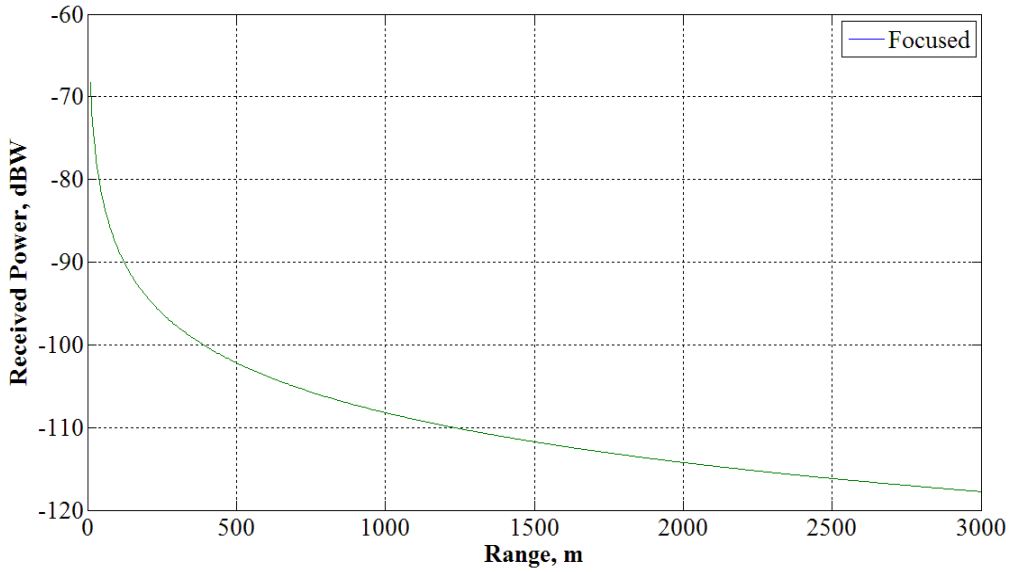

Figure 15. Plot of power signal at receiving PRR for a single transmitting PRR.

Comparing Figures 13 and 15, the received power P_r at a PRR is 6 dB lower than at the base station. This is due to a higher gain at the vehicle base station antenna. Since the minimum received power at a PRR is of lower sensitivity, it will serve as a threshold value in order for successful communication to take place.

Figure 16 shows the received power beam pattern plot for a single PRR at 800 m. From the plot it can be seen that all the values are constant which means that any point on the plot is equal to –106.28 dBW from Figure 15.

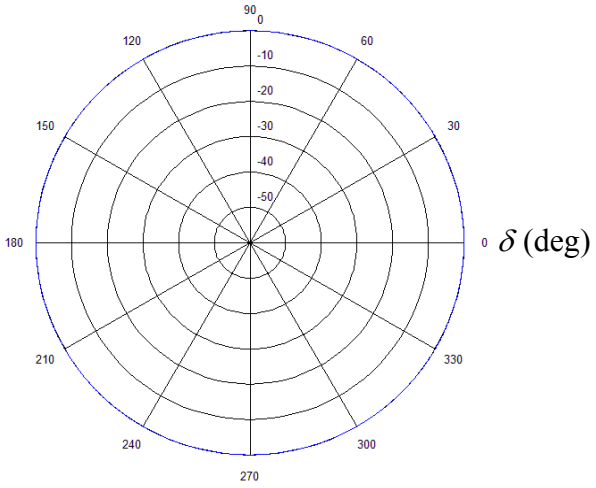

Figure 16. Normalized plot of received power focused at range of PRR for a single transmitting PRR with d_1=800 m.

3. Communication between Three PRRs and Vehicle Base Station

The configuration of three PRRs and vehicle antenna (base station) is created based on the mission operational plan. Usually, a group of three soldiers form a unit for dismounted operation. This model is created with a clear path between the PRRs and vehicle antenna (line of sight) with no multipath fading, phases coherently synchronized and fully compensated. Figure 17 shows the scenario configuration. In this scenario, the distance between the PRRs and the vehicle base station is set to range distances d_n and displacement distances p_n to analyze the effects on beamforming and its applicability.

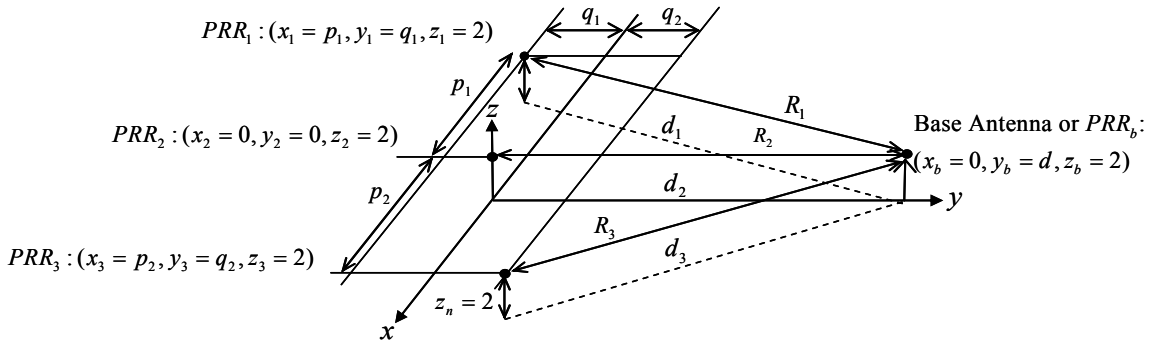

Figure 17. Three PRR configuration with PRR_1 at $(x_1 = p_1, y_1 = q_1, z_1 = 2)$, PRR_2 at $(x_2 = 0, y_2 = 0, z_2 = 2)$ and PRR_3 at $(x_3 = p_2, y_3 = q_2, z_3 = 2)$, and base station at $(x_b = 0, y_b = d = d_2, z_b = 2)$ in meters.

a. Soldier Displacement Distances at 5 m apart, Range Distances at 400 and 800 m

The displacement distance between the soldiers is kept to $p_1 = p_2 = 5$ m in line with operation tactics and $q_1 = q_2 = 0$ m. Thus the three PRRs form a linear array on the *x* axis. Applying beamforming, Figures 19 and 20 show the total received powers P_r from the three PRRs as a function of distance along the *y* axis. In Figure 18, the collective beam is focused at 400 m. In Figure 19 the beam is focused at 800 m. The total received power signal P_r when focused at the base station is –84.74 dBW and –90.74 dBW at 400 and 800 m. The plane wave scanning plot is obtained when the phases to focus the beam at infinity are used. In this case, to scan the beam broadside to the array axis (*y* direction), the phase shifts are all 0 degrees. It can be seen from both plots that the maximum received power is attained with the beam focused compared to plane wave scanning.

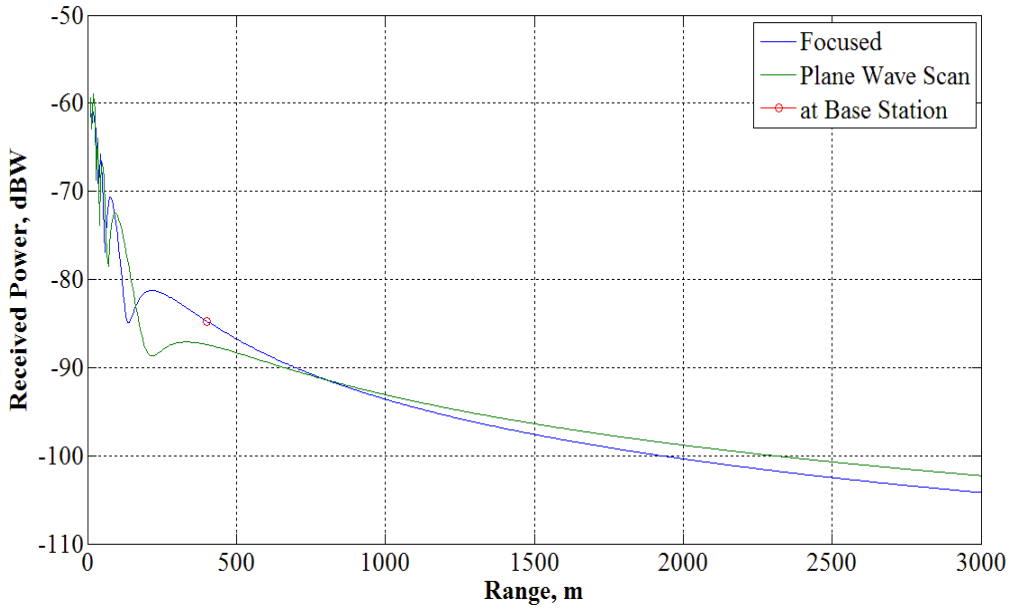

Figure 18. Plot of power signal received at base station for three transmitting PRRs at range distance 400 m and displacement distances at 5 m.

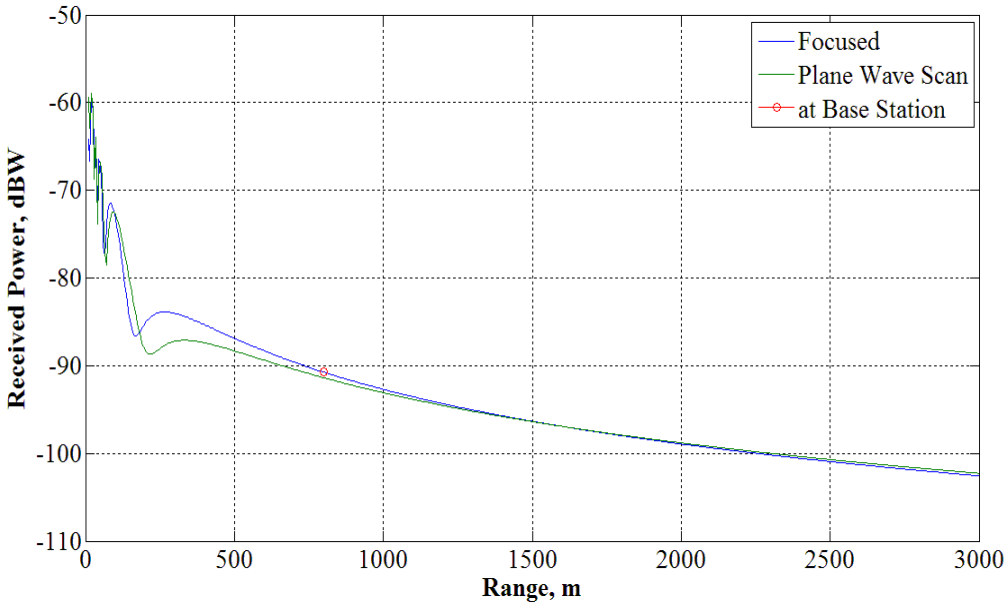

Figure 19. Plot of power signal received at base station for three transmitting PRRs at range distance 800 m and displacement distances at 5 m.

Figures 20 and 21 show the difference between the focus and plane wave scanning cases for distances of 400 and 800 m, respectively. From the plots, it can be seen that there is a large fluctuation at short distances (lower than 215 m). This means that any small shift in distance results in large variation in received power values attained from focusing versus plane wave scanning. Only at longer focusing distances (about 800 m and above) does the variation becomes negligible. This is where the far field boundary is approached.

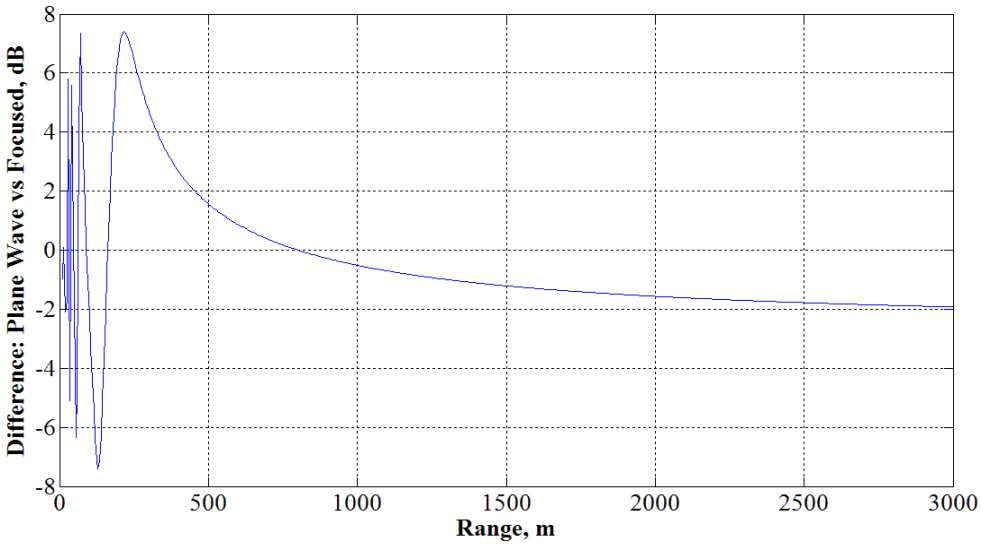

Figure 20. Plot of difference between plane wave versus focused powers for base station at 400 m and displacement distances at 5 m.

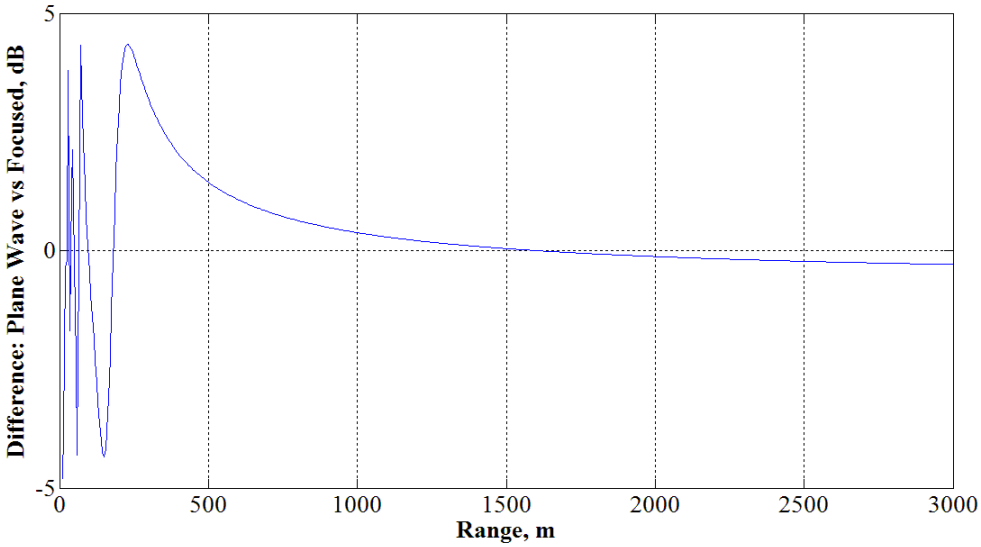

Figure 21. Plot of difference between plane wave versus focused powers at range of base station at 800 m and displacement distances at 5 m.

Figures 18 and 19 show that there is a power gain increase of 9.5 dB with beamforming compared to the individual PRR configuration shown in Figure 13. In terms of the minimum received power of –94.27 dBW and –100.29 dBW obtained from the

benchmark calculations, the achievable communication range increased by 300% from 400 m to 1200 m and from 800 m to 2400 m. This is for clear line of sight conditions. This fulfills the expression in Equation (3-40) where the distance increases by *N*.

Figures 22 and 23 show the plots of the received power patterns at the focus range for three PRRs. That is, the pattern is taken in a circle with the same range as the base station, which is not necessarily in the far field. The pattern angle, δ, is defined in Figure 6. From both plots, it can be seen that the maximum is achieved at 0 degrees with the main lobe of the radiation pattern pointing towards 0 degrees which is the location of the vehicle base station which corresponds to –84.74 dBW and –90.74 dBW at 400 and 800 m. The half-power beam width is found to be 0.44 degrees from both plots.

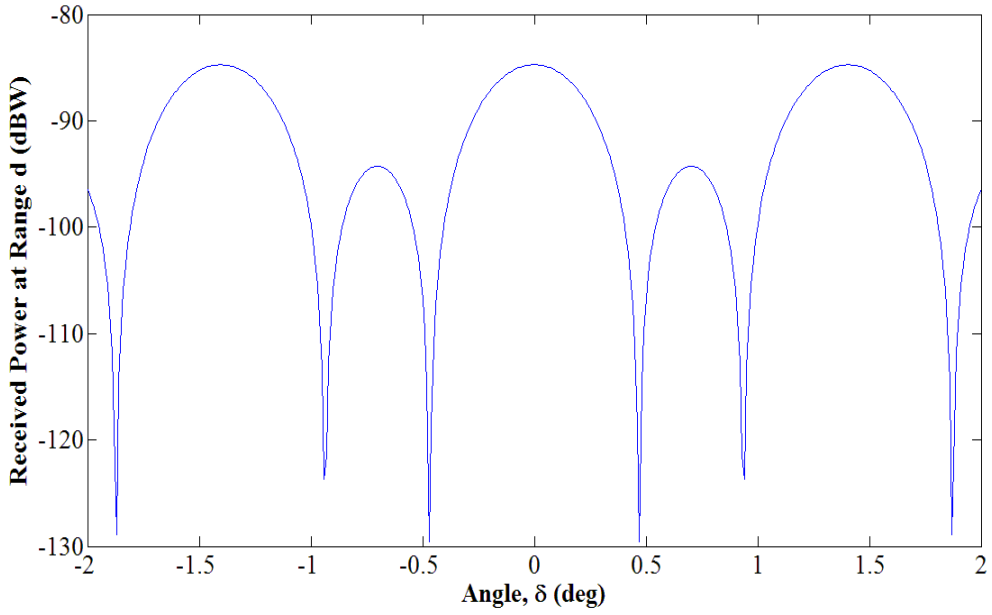

Figure 22. Plot of received power beam pattern focused at base station for three transmitting PRRs at range distance 400 m and displacement distances at 5 m.

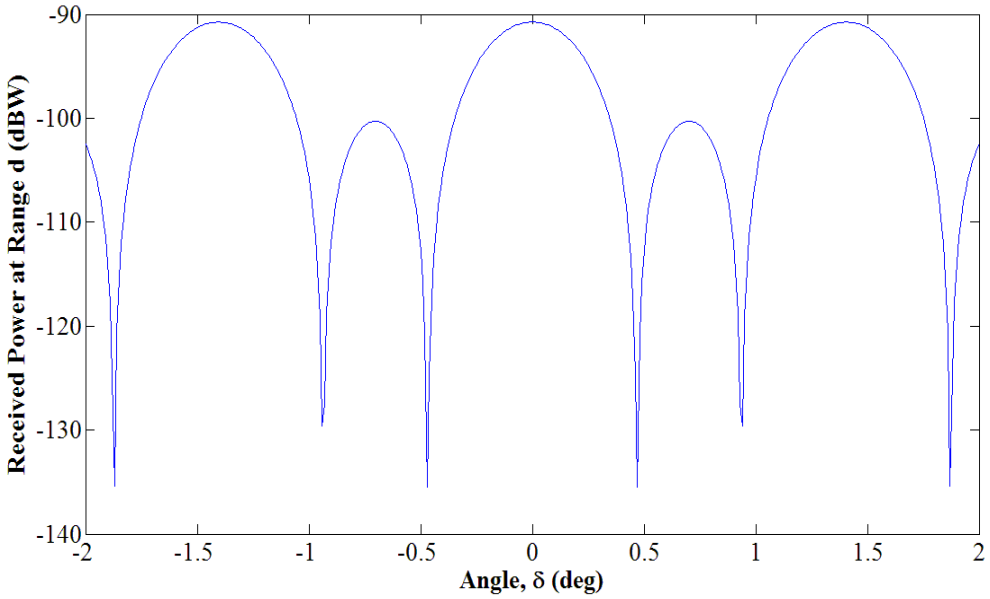

Figure 23. Plot of received power beam pattern focused at base station for three transmitting PRRs at range distance 800 m and displacement distances at 5 m.

b. Soldier Displacement Distances at 5 m apart, Range Distances at 1200 and 2400 m

With beamforming, the range of communication can be increased substantially. The next configuration is set to range distances of 1200 and 2400 m to analyze the effects of beamforming and its applicability at these distances. The displacement distance between the soldiers is kept at 5 m in line with operation tactics. At 5 m, the dimension of the PRR array becomes L=10 m.

Figures 24 and 25 show the respective received power pattern plot when the PRRs are focused at ranges of 1200 and 2400 m. From the plots it can be seen that the maximum is achieved at 0 degrees and thus the main lobe of the radiation pattern points towards the vehicle base station. This means that the received power signal at 0 degrees is –94.27 dBW and –100.29 dBW for distances 1200 m and 2400 m, respectively. The half-power beam width for both distances is found to be about 0.44 degrees. The small beamwidth means that the location accuracy of the PRRs and base station are crucial to focus the main lobe beam in direction for efficient beamforming.

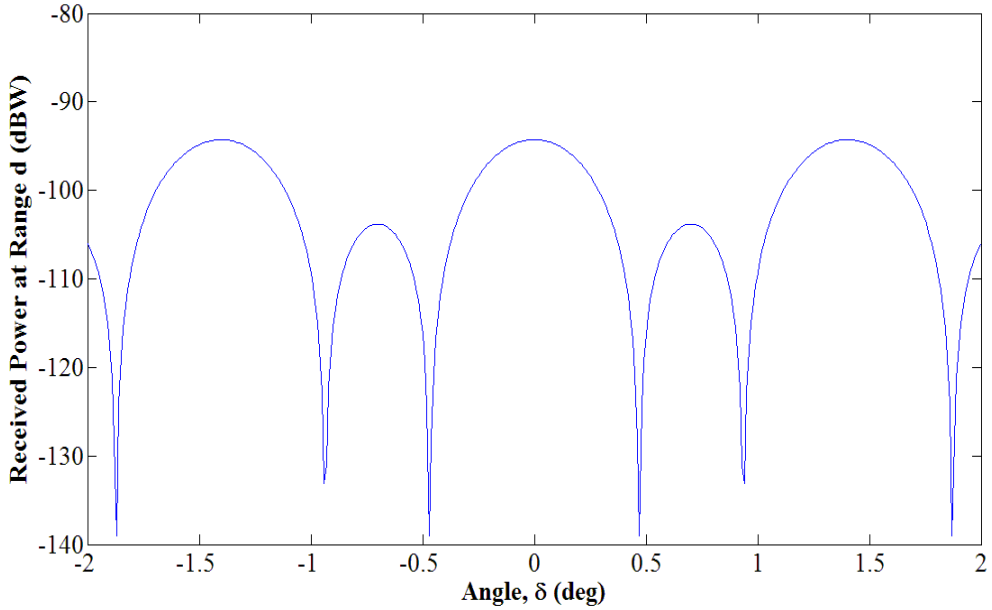

Figure 24. Plot of received power beam pattern focused at base station for three transmitting PRRs at range distance 1200 m and displacement distances at 5 m.

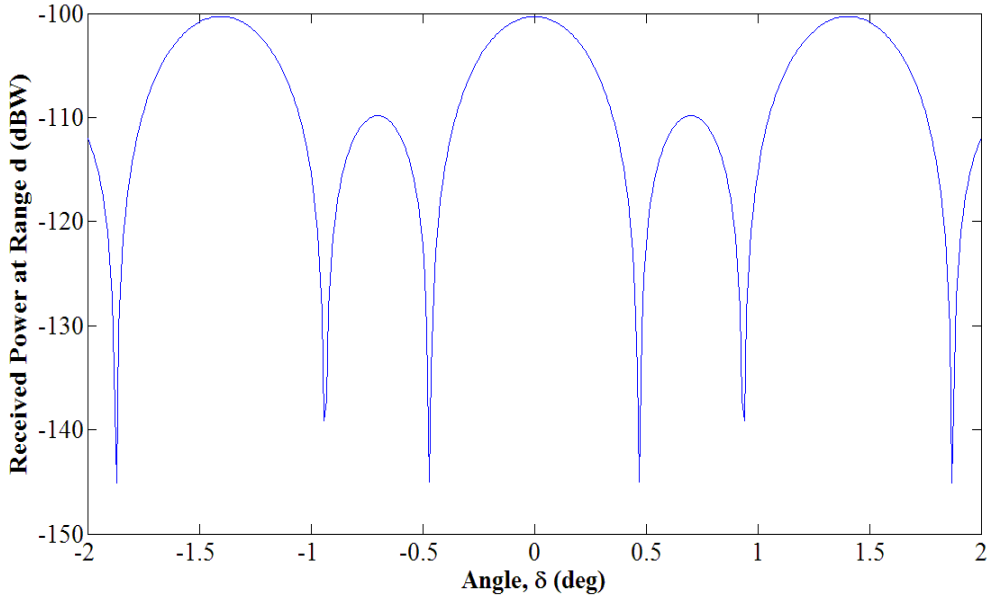

Figure 25. Plot of received power beam pattern focused at base station for three transmitting PRRs at range distance 2400 m and displacement distances at 5 m.

c. Soldier Displacement Distances at 20 m apart, Range Distances at 400 and 2400 m

In this scenario, the displacement distance between the soldiers is increased to 20 m so that deployment distance is lengthened. This configuration is to analyze the effects on beamforming and its applicability at longer soldier displacement distances. At 20 m, the dimension of the array becomes L=40 m.

Figures 26 and 27 show the difference between the beam focused and plane wave scanning for range distances 400 and 2400 m, respectively. From the plots, it can be seen that there is a large fluctuation at distances below 1150 and 1400 m, respectively. This means that any small shift in distance results in a large variation in received power values obtained from focused versus plane wave scanning. Only at larger distances do the fluctuations become lower.

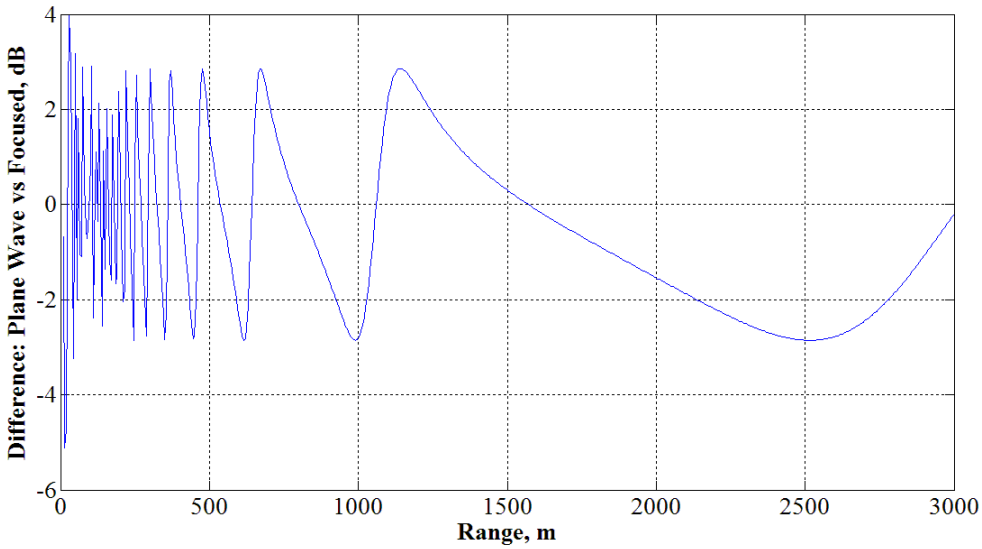

Figure 26. Plot of difference between plane wave versus focused powers for base station at 400 m and displacement distances at 20 m.

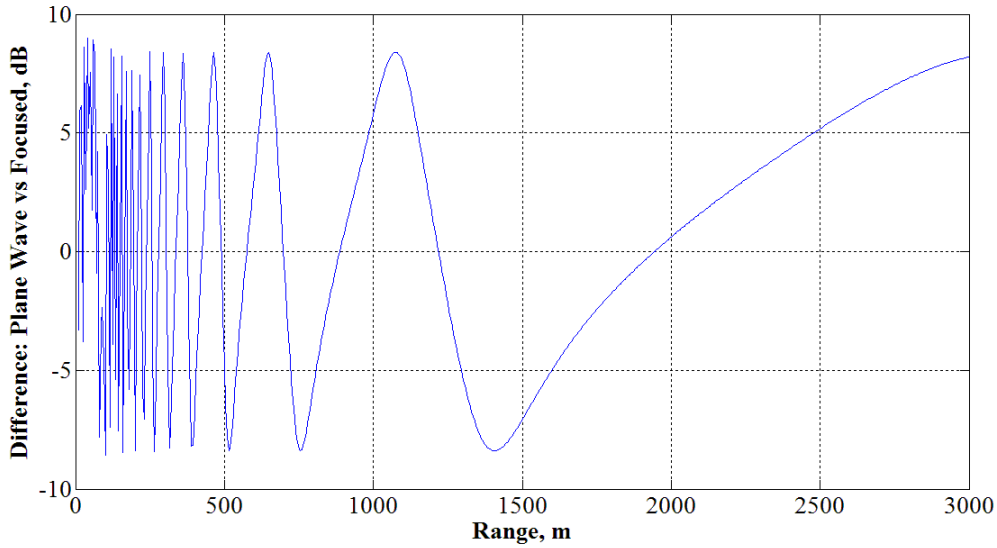

Figure 27. Plot of difference between plane wave versus focused powers for base station at 2400 m and displacement distances at 20 m.

Figures 28 and 29 show the plots of the received power pattern focused for three PRRs at range distances 400 and 2400 m, respectively. From both plots, it can be seen that the maximum is achieved at 0 degrees with the main lobe of the radiation pattern pointing towards 0 degrees which is the location of the vehicle base station which corresponds to –84.74 dBW and –100.29 dBW at 400 and 2400 m. The half-power beam width is found to be 0.11 degrees from both plots which is very narrow and therefore it will be difficult to focus the beam accurately.

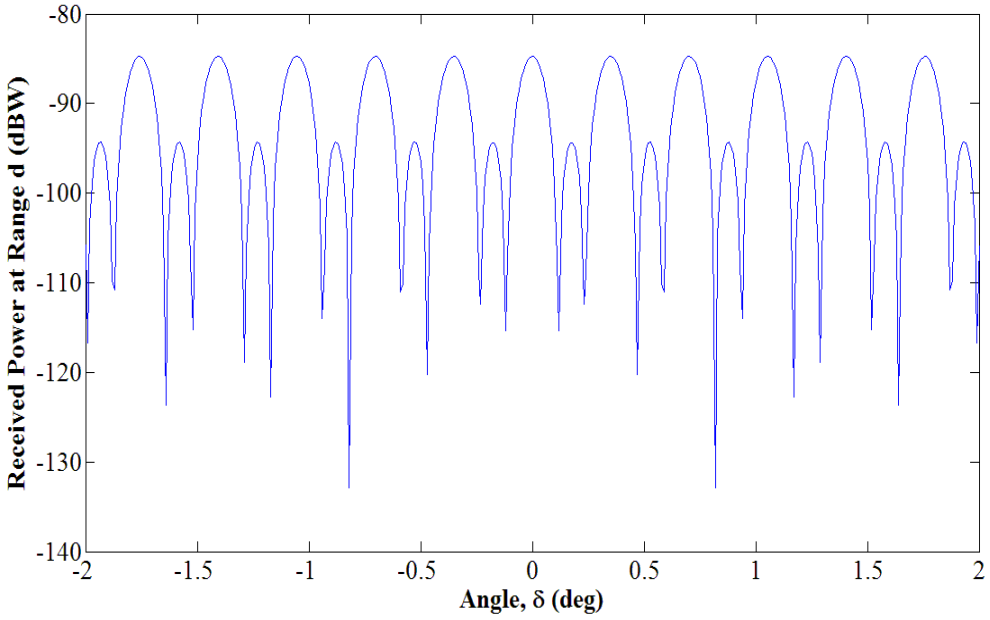

Figure 28. Plot of received power beam pattern focused at base station for three transmitting PRRs at range distance 400 m and displacement distances at 20 m.

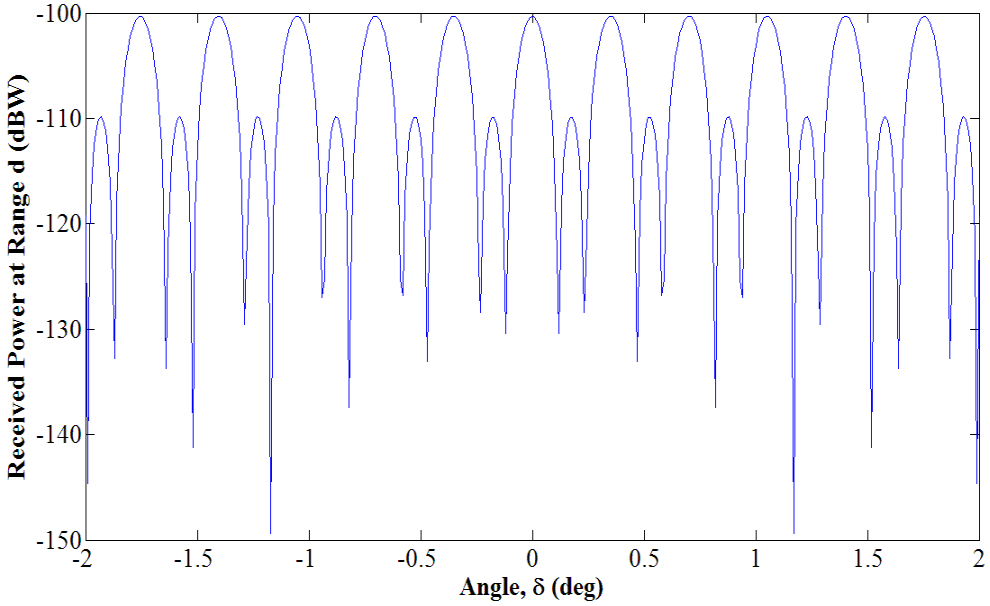

Figure 29. Plot of received power beam pattern focused at base station for three transmitting PRRs at range distance 2400 m and displacement distances at 20 m.

d. Soldier Displacement Distances at p_1=20 and p_2=5 m apart, Range Distances at 400 and 2400 m

In this scenario, the displacement distances between the soldiers are specified differently at 20 and 5 m. This configuration is to analyze the effects on beamforming and its applicability at different soldier displacement distances. At 20 and 5 m, the dimension of the PRR array becomes L=25 m.

Figures 30 and 31 show the difference between the beam focused and plane wave scanning at ranges 400 and 2400 m, respectively. From the plots, it can be seen that there is a large fluctuation at distances below 1150 and 1400 m, respectively. This means that any small shift in distance result in large variation in received power values attain from focus at range and plane wave scanning. Only at longer distance are the fluctuations lower.

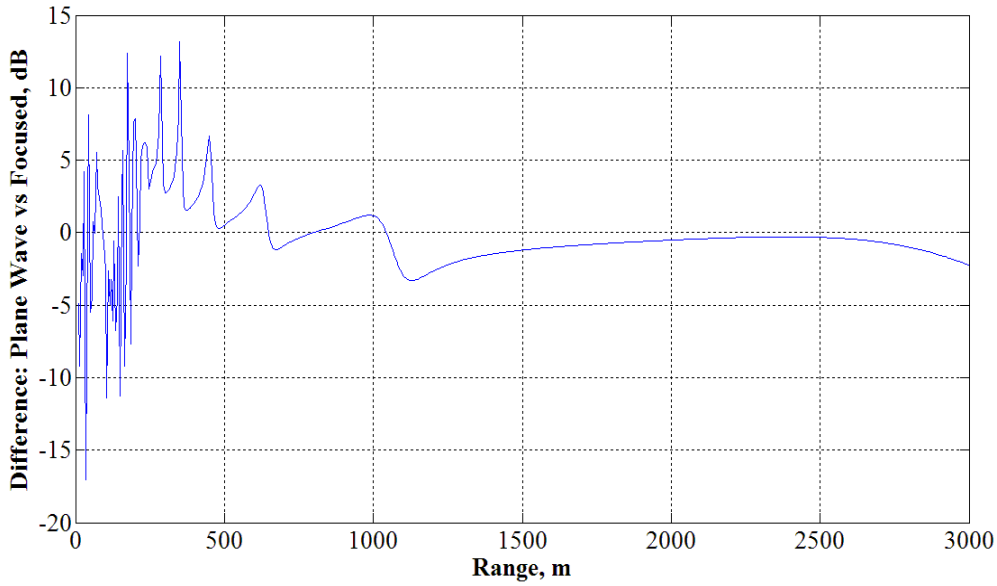

Figure 30. Plot of difference between plane wave versus focused powers for base station at 400 m and displacement distances at $p_1 = 20$ and $p_2 = 5$ m.

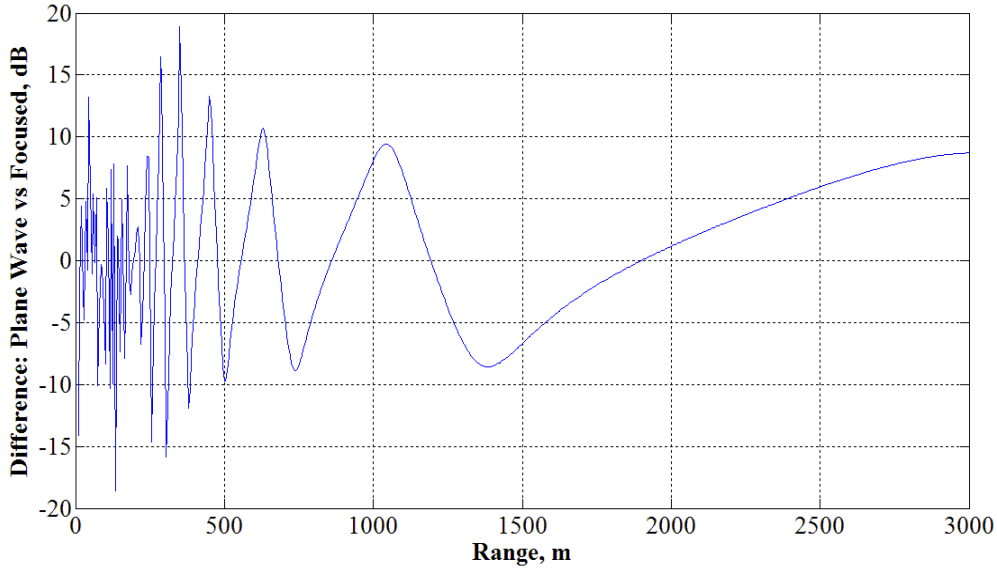

Figure 31. Plot of difference between plane wave versus focused powers for base station at 400 m and displacement distances at $p_1 = 20$ and $p_2 = 5$ m.

Figures 32 and 33 show the plots of the received power pattern at the focus range for three PRRs at range 400 and 2400 m. From both plots, it can be seen that the maximum is still achieved at 0 degrees with the main lobe of the radiation pattern pointing towards 0 degrees which is the location of the vehicle base station. The power levels are –84.74 dBW and –100.29 dBW at 400 and 2400 m. The half-power beam width is found to be 0.16 degrees from both plots which is very narrow and therefore it will be difficult to focus the beam accurately.

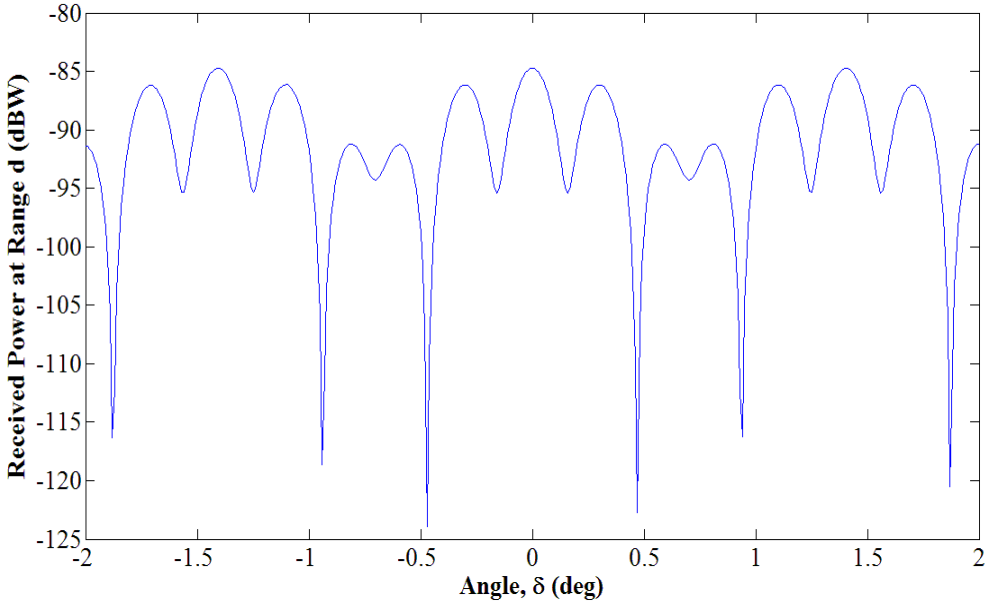

Figure 32. Plot of received power beam pattern focused at base station for three transmitting PRRs at 400 m and displacement distances at $p_1 = 20$ and $p_2 = 5$ m.

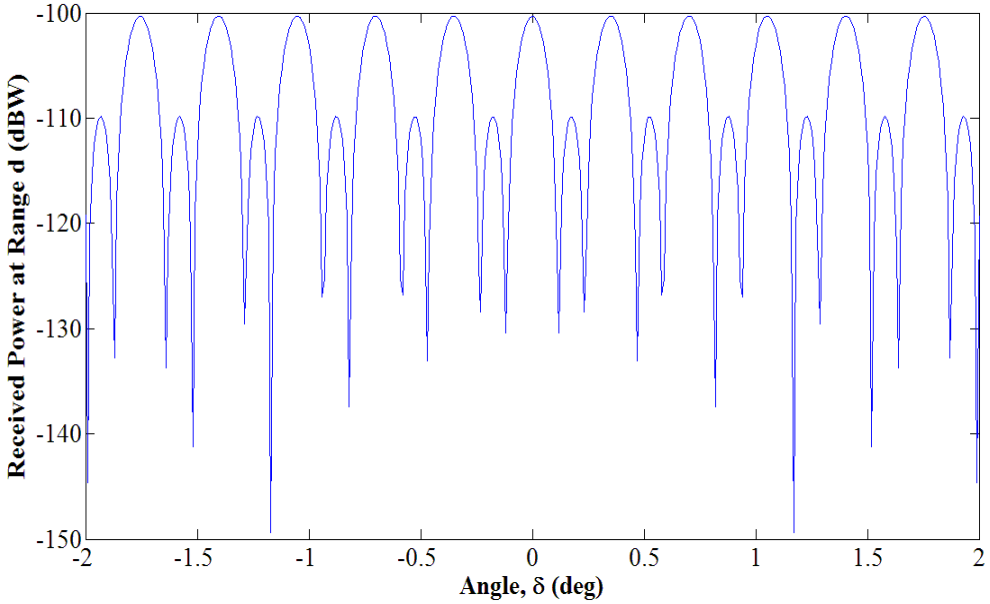

Figure 33. Plot of received power beam pattern focused at base station for three transmitting PRRs at 2400 m and displacement distances at $p_1 = 20$ and $p_2 = 5$ m.

e. Soldier Displacement Distances at p_1=20 and p_2=5 m apart, Range Distances at d=400 m with q_1= q_2=5 m

In this scenario, the displacement distances between the soldiers are 20 and 5 m respectively. PRR_1 is at a distance 5 m further from the base station at q_1=5 m and PRR_3 is at a distance 5 m closer to the base station at q_2=5 m. This configuration is to analyze the effects on beamforming and its applicability with range and displacement distances. At displacement distance of 20 and 5 m, the dimension of the array becomes L=27.69 m.

Figure 34 shows the difference between beam focusing and plane wave scanning at base station range. From the plot, it can be seen that there is a large fluctuation at distances below 1380 m. This means that any small shift in distance results in large variation in received power values attained from focus at range and plane wave scanning. Only at longer distances above 1380 m do the fluctuations become lower.

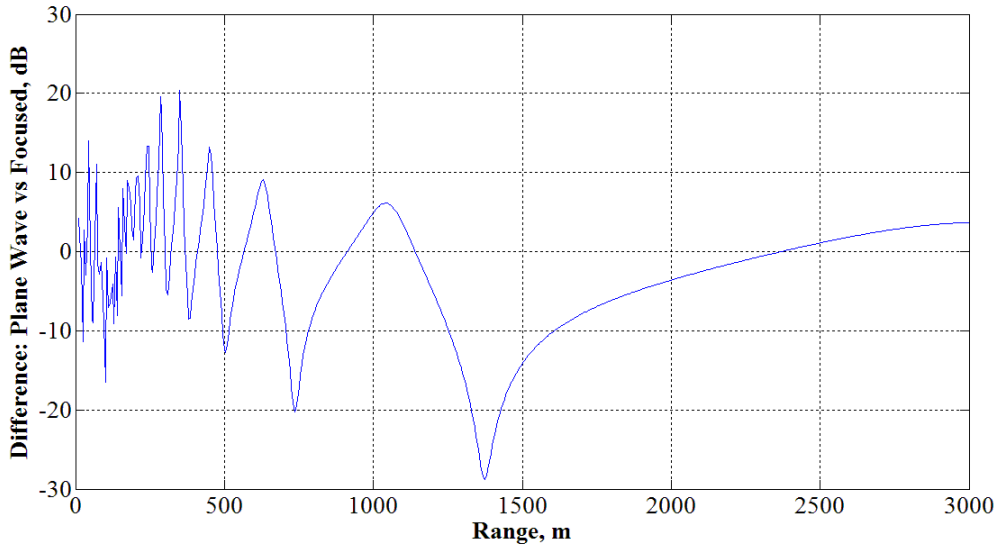

Figure 34. Plot of difference between plane wave versus focused powers at base station, range distances at $d = 400\,\text{m}$, $q_1 = q_2 = 5\,\text{m}$ and $y_2 = 0$ m, and displacement distances at $p_1 = 20$ and $p_2 = 5$ m.

Figure 35 shows the plot of the received power pattern focus at range for three PRRs focused at 400 m. It can be seen that the maximum is still achieved at 0 degrees with the main lobe of the radiation pattern pointing towards 0 degrees which is the location of the vehicle base station. The power level is –84.74 dBW. The half-power beam width is found to be 0.16 degrees from the plot implying it is difficult to focus the beam accurately.

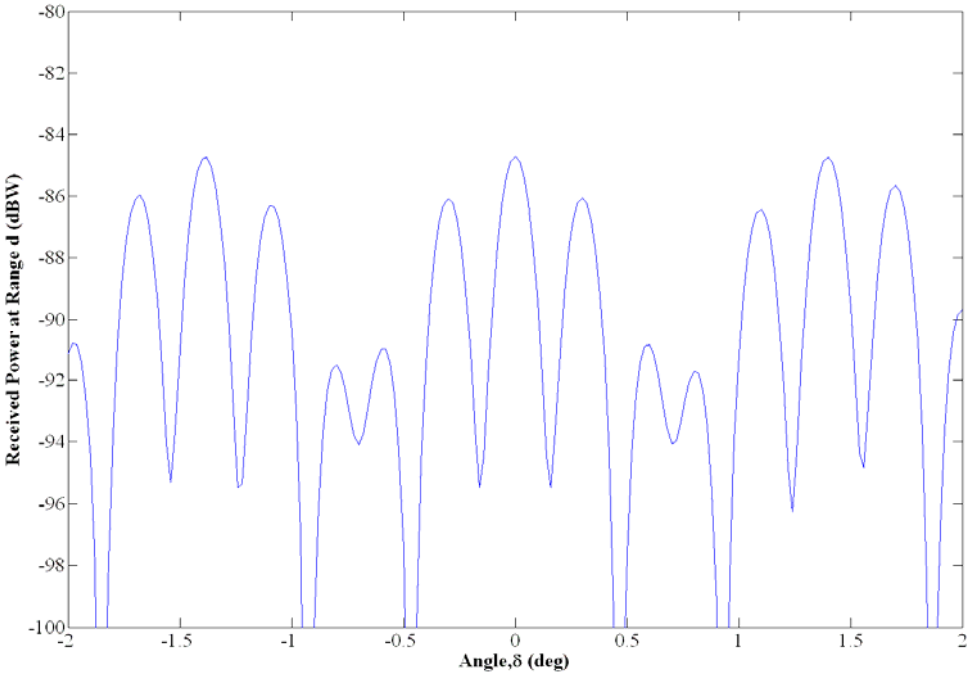

Figure 35. Plot of received power beam pattern focused at base station distance of $d = 400\,\text{m}$, $q_1 = q_2 = 5\,\text{m}$, $y_2 = 0$ m and displacement distances at $p_1 = 20$ and $p_2 = 5$ m.

f. Beamwidth and Received Power Variation along Designated Path

In this scenario, PRR_1 is moved along a designated path as shown in Figure 36. This is to study the effects of the beamforming performance in terms of beam width and received power. In this configuration, PRR_2 is fixed at ($x_2 = 0$ m, $y_2 = 0$ m)

and PRR_3 is fixed at ($x_3 = 0$ m, $y_3 = -5$ m) while PRR_1 is moved along the path. The base station is at ($x_b = 0$ m, $y_b = 400$ m). All the PRRs and base station antennas are assumed at equal height.

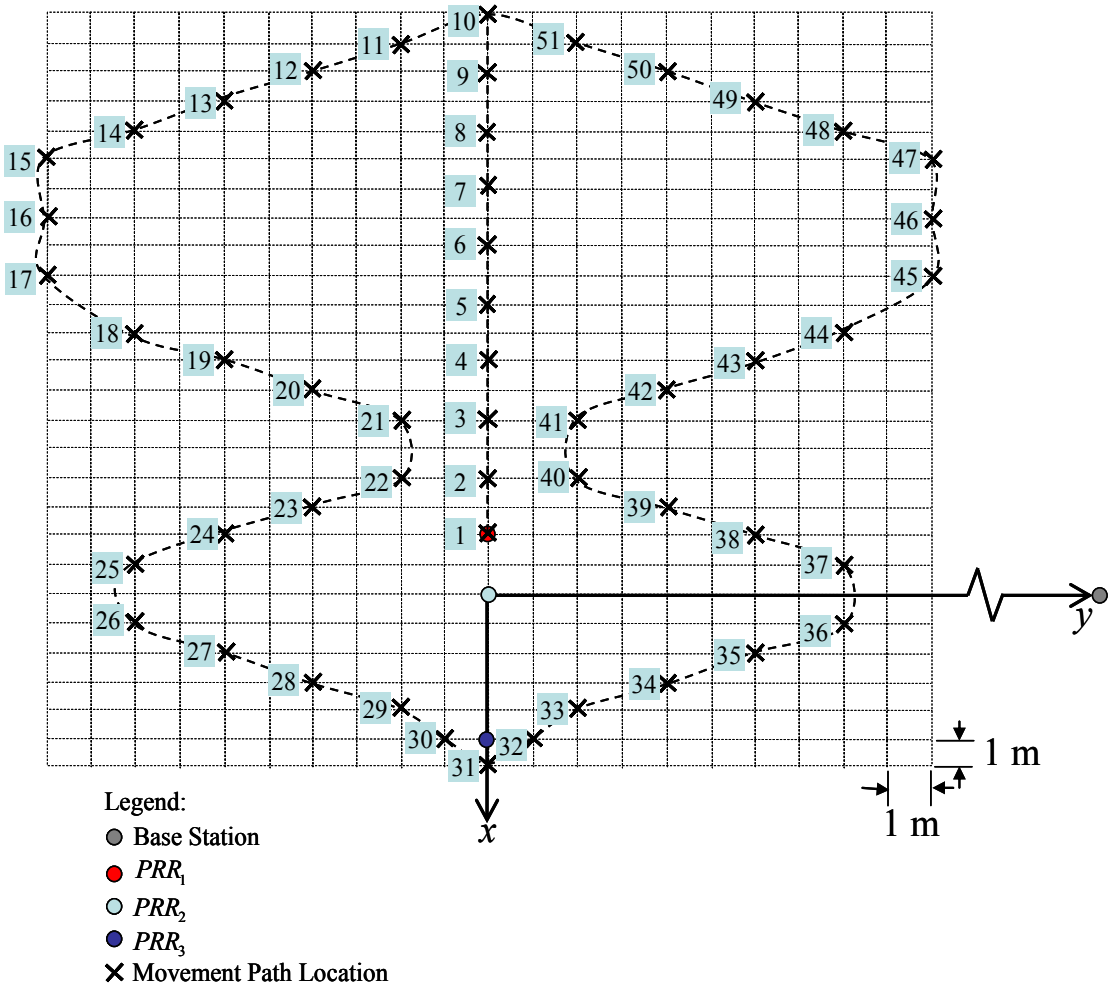

Figure 36. PRR_1 designated movement path.

Figure 37 shows the plot of beamwidth and received power when all three PRRs focus at base station while PRR_1 moves along the designated path shown in Figure 36. From the plot, it can be seen the received power is highest and constant when PRR_1 is in line with PRR_2 and PRR_3. However, the beamwidth gets smaller when the dimension

of the array L gets larger. The highest beamwidths, above 0.6 degrees, occur when PRR_1 is within 2 m of the other two PRRs on the y axis. When PRR_1 is furthest from the base station, the received power is lowest. When PRR_1 is at the locations which are symmetrical, i.e. locations 22 and 40, the beamwidths and received powers are similar. The beamwidths can be seen to be less than 0.9 degrees hence it will be difficult to focus the beam accurately. The variation in power is less than 1 dB over the entire path.

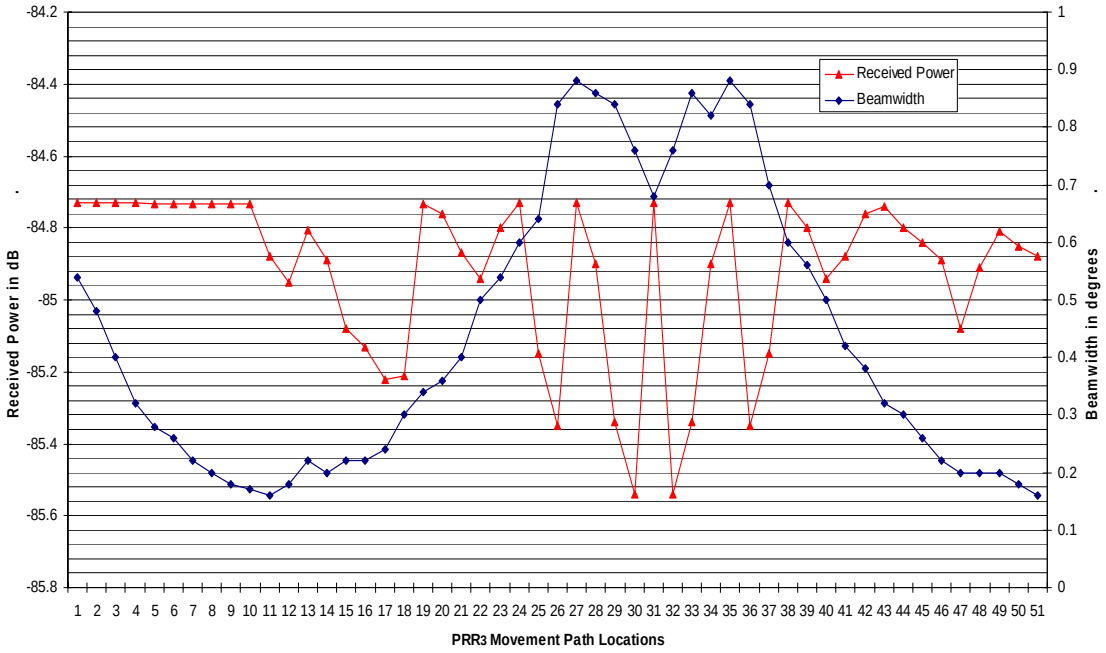

Figure 37. Received power and beamwidth with PRR_1 movement along designated path with beam focused at range 400 m.

4. Communication between Three PRRs and a Single PRR

The results are similar to those obtained in Section III.C.3.a for communication between three PRRs and vehicle base station, where the only difference is the 6 dB in received power due to the higher antenna gain at the vehicle base station. The scenarios can be assumed similar to those obtained in Section III.C.3.a to g but with 6 dB lower gain and are not repeated here.

D. SUMMARY

This chapter presented some concepts in electromagnetics that are relevant to distributed beamforming. The rationale and simulation model for the distributed beamforming was described. Following which, the results of the simulations were presented. Finally, the benefits and limitations of beamforming for the different scenarios were discussed. Findings showed that beamforming can be applied for all the specified scenarios with some range improvements realized. However, the small half power beam width means that the locations of the PRRs and receiving antenna must be very accurate to focus the beam in the correct direction for efficient beamforming and reap the benefit of higher range operations.

Next chapter will study the environment and seasonal effects pertaining to foliage on beamforming.

IV. TERRAIN WITH FOLIAGE

This chapter begins by describing the foliage environment effects on wave propagation. Next, the rationale, considerations and assumptions on modeling of the foliage environment are presented. Following which, simulations with Matlab to assess the foliage effects on the adopted beamforming strategies are performed. A tradeoff study on the performance with recommendations for field operation concludes this chapter.

A. FOLIAGE ENVIRONMENT

Forested environments can affect wireless communication significantly. It affects the communication channel significantly and imposes constraints on the system parameters. The leaves and branches of tree offer significant attenuation to UHF and microwave signals. The most important effect introduced by the forest is the excess signal attenuation in addition to that of free-space path loss introduced by wave propagation. The signal attenuation by foliage is mainly caused by the absorption and scattering by discrete scatterers such as branches and leaves within the forest. Attenuation depends on the frequency and on the type of tree through the size, shape, and angular distribution of the leaves and branches. Foliage attenuation is considered one of the dominant effects for rural and suburban areas. [19-22]

Measurements of transmission loss at 869 MHz for low elevation angles through the canopies of large isolated trees found attenuations of 10 dB or more. For these measurements an average specific attenuation α_{dB} was found to be 1.1 dB/m. [23]

In another example, the specific attenuation for distances up to 20 m extracted from measurements at 11.2 GHz in an apple orchard are α_{dB} = 2.0 dB/m when the trees are in leaf and 1.7 dB/m when the trees are without leaves. [24]

B. FOLIAGE ENVIRONMENT MODELING CONSIDERATIONS

In addition to the problem of characterizing individual types of trees, modeling the effects of trees is complicated by the many ways they are grouped in and around metropolitan areas. At one extreme is a natural dense forest in which the trees form a

continuous canopy whose top is nearly flat. In distant suburbs and urban parks, the density of trees may be less than in a forest, so the canopy will be broken. [24]

1. Foliage Propagation Consideration

Treating the leaves and branches as a random medium, the attenuation can be evaluated theoretically. Within the random medium, the total fields consist of a coherent part and a diffuse part. The coherent fields are associated with the forward scatter past the individual leaves and branches. The diffuse fields are those resulting from scattering away from the forward direction. As the radio waves propagate into the random medium, the coherent fields are initially dominant. The fields decay relatively rapidly as a result of absorption in the leaves and branches. This is due to scattering into the diffuse fields. After several nepers of decay of the coherent fields, the diffuse fields become dominant and continue to decay, but at a much lower rate. [24]

Foliage propagation models treat the forest as an effective lossy dielectric medium which predict an exponential increasing of path-loss with respect to the propagation distance within the forest. Such a model captures only the coherent power of the signal which comes from the mean electromagnetic field propagating through the forest and neglects the diffuse power from the field fluctuation due to the random distribution of the scatterers, such as branches and leaves, within the forest. However, such incoherent power tends to dominate the overall receive power after a certain distance because of the exponential-decaying behavior of the coherent power especially in a long-distance communication system such as satellite communications. [20]

In this study, the model will only consider the coherent power of the propagating signal due to the relative short communication range of the PRR system.

2. Statistical Analysis on Propagation Wave Paths

In the presence of a tree between a transmitter and receiver, the propagated wave may reach the receiver via a number of paths. For example as shown in Figure 38, one or more could be through the tree, another could be diffracted from the top, others may be due to lateral diffraction, etc. Each of the paths taken will eventually result in a length

that is different from that of the other paths. The phase of a signal received from one path will be different from the phase of a signal received from another path. [25]

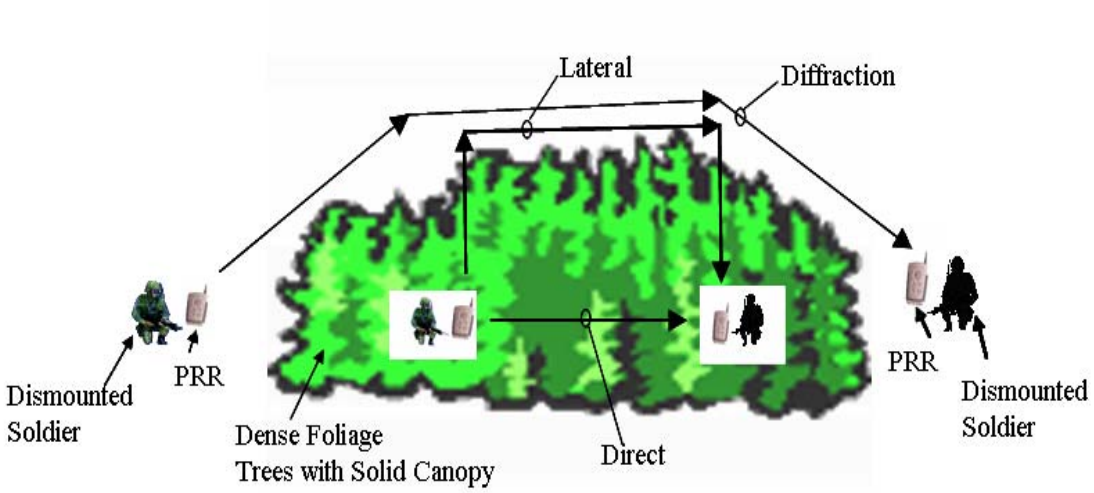

Figure 38. Propagation wave paths in terrain with foliage.

In [24], a first order statistical analysis of the received signal was performed to compute the Cumulative Distribution Function (CDF) of the normalized received signal with respect to the trend across the frequency band of interest. The results demonstrate the lognormal nature of the fading characteristics of the signal strength in the shadow of a deciduous tree.

In general, the many randomly positioned branches and a number of randomly oriented leaves will be diverse and will vary in thickness, shape, electrical properties and differ in their number. The scenario can be represented by a direct signal passing through a cascade of attenuators. The distribution of the direct signal will depend upon the number of attenuators, which is assumed to increase with an increase in frequency. As the frequency increases, the number of branches and leaves have a greater effect on the signal received as their physical size approximates the wavelength of the transmitted

signal. This results in a higher probability of signal attenuation. Since the large numbers

of attenuators are independent, by means of the central limit theorem, their contribution will tend to be Gaussian distributed. [25]

3. Propagated Wave and Tree Modeling Assumptions

It is assumed that at each receiving location, the transmitted wave will eventually reach the receiver antenna after propagating through many randomly positioned branches and a number of randomly oriented leaves.

Trees, because of their natural growth, possess an inherent symmetry giving them the shape of an umbrella. A simple geometrical representation, based on the visual shape of a deciduous tree, by means of an elliptical parabolic and an elliptical conical section is used as the model. Such a representative model would include most of the tree canopy. In [25], data were collected for various penetration depths versus antenna receiver position within the shadow of the tree to obtain empirical formulas.

4. Seasonal Effects on Propagation Loss

Seasonal effects contribute to the already difficult task of characterizing individual types of trees and how they grouped. Seasonal changes affect the type of tree through the size, shape, and angular distribution of the leaves and branches, thus also the electromagnetic field propagating through the forest.

In [25], the study was directed to categorize a specific tree analysis, a deciduous type commonly found near European roadside. The study was based on the results of an experimental field campaign conducted in Spring/Summer and Autumn/Winter. Various spatial positions along the shadow of a mature deciduous tree with and without leave readings at different foliage depths were recorded. Figures 39 and 40 show a deciduous tree in Spring/Summer with leaves and Autumn/Winter without leaves, respectively. The study included determining typical tree attenuation caused by shadowing with respect to line of sight for both cases of trees with and without leaves in order to assess the leaf cover. The path loss versus frequency as a function of foliage effects is used as the model in the simulations in this study [25].

Figure 39. Deciduous tree in Spring/Summer with leaves. (From [26])

Figure 40. Deciduous tree in Autumn/Winter without leaves. (From [27])

5. Differential Attenuation

It is assumed that the direct ray is the dominant component of the field strength received in the shadow of the tree. The received power is exponentially related to the tree depth traversed. Table 5 shows the differential attenuation constants due to seasonal effects. The differential attenuation increases with an increase in the frequency. The increase of the differential attenuation is a power dependence of the form:

$$\alpha = af^b \tag{4-1}$$

where α is differential attenuation in decibels per meter, a and b are constant from different seasonal characteristics, and f is the frequency expressed in GHz. [25].

Table 5. Differential Attenuation Propagation Characteristics. (After [25])

Season	Summer			Winter		
Parameters	Median	50%	90%	Median	50%	90%
a	0.57	0.71	0.78	0.36	0.52	0.59
b	0.60	0.47	0.42	0.43	0.29	0.25

6. Excess Path Loss Model

Modeling the propagation path loss through tree foliage is very complicated. The attenuation due to foliage is a function of many parameters that combine to influence the propagation phenomena in this type of environment. These parameters include height, foliage density, type of tree, and seasonal variations. In addition, receiver antenna height with respect to the tree height, path length, position with respect to the tree height, path length, position with respect to the tree, terrain features, polarization and frequency, all combine to make quantitative prediction difficult. However, a theoretical approach was used to successfully predict the path loss. [25]

The theoretical approach was to measure the received powers along the shadow of the tree and without the presence of the tree (line of sight). The difference given by subtracting the receiving power with path loss from the receiving power without path loss will be the excess path loss due to foliage.

The excess path loss can be expressed using the exponential decay model by

$$L_e = \alpha d_f \tag{4-2}$$

where d_f is the depth of a deciduous tree. Therefore, Equation (3-31) including the decay model becomes

$$E_b = \sum_{n=1}^{N} \sqrt{\frac{2\eta_0 P_n G_n(\theta_n)\left|F_n(\theta)\right|^2}{4\pi {R_n}^2}} e^{-jkR_n} e^{j\Phi_n} e^{-\alpha_n d_{f_n}} \hat{e}_n \bullet \hat{h}_b$$
$$= \sum_{n=1}^{N} \sqrt{\frac{2\eta_0 P_n G_n(\theta_n)\left|F_n(\theta)\right|^2}{4\pi {R_n}^2}} e^{-jkR_n} e^{j\Phi_n} e^{-\alpha_n d_{f_n}} \quad (4\text{-}3)$$

where $\hat{e}_n \bullet \hat{h}_b \approx 1$ since all antennas are parallel and $e^{-\alpha_n d_{f_n}}$ is the attenuation term due to foliage at each individual PRR element. Alternatively the loss factor could be included in the path gain factor F_n. In the foliage study ground reflections are ignored so $\left|F_n\right| = 1$. The insertion phase of the attenuation medium has also been neglected.

C. MATLAB SIMULATION

Matlab by Mathworks is the simulation and analysis tool used to study the foliage environment effects. Field operation scenarios modeled in Chapter III.C are applied here to study the effects of foliage attenuation on the beamforming strategies and on operations. Analysis of the simulation results will be presented and discussed.

1. Differential Attenuation Model

Figures 41 and 42 show the plot of differential attenuation versus frequency for summer and winter, respectively. It can be seen clearly that the differential attenuation increases with frequency. Comparing both figures, the differential attenuation during summer is greater than during winter. This means that trees with foliage introduce greater attenuation than trees without foliage. This is due to the fact that during the autumn/winter season the tree is composed only of dry branches and twigs; therefore the content of water inside is low and has lesser effect on the propagating waves. On the other hand, during spring/summer season, branches have higher content of water which introduces greater attenuation effects on the propagation waves. [25]

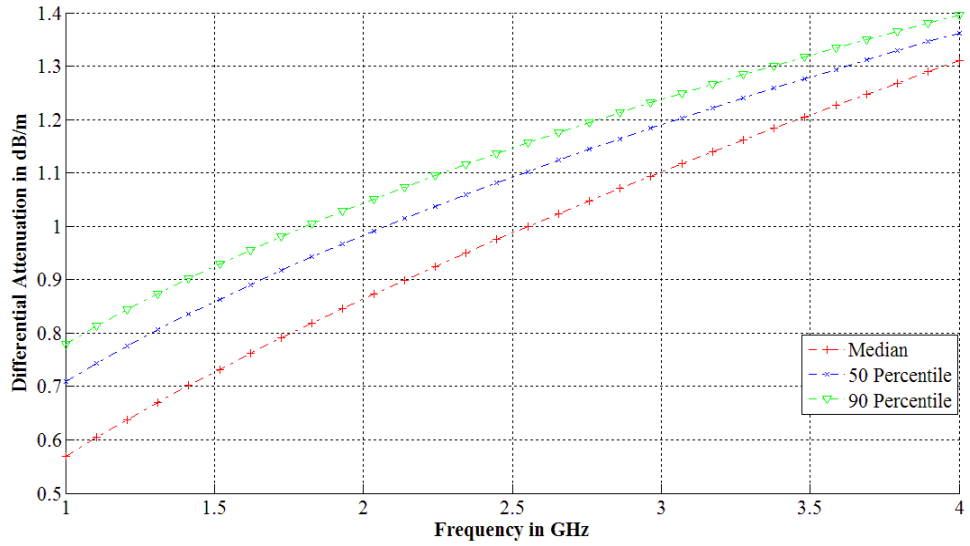

Figure 41. Differential attenuation versus frequency, tree with foliage (summer). (After [25])

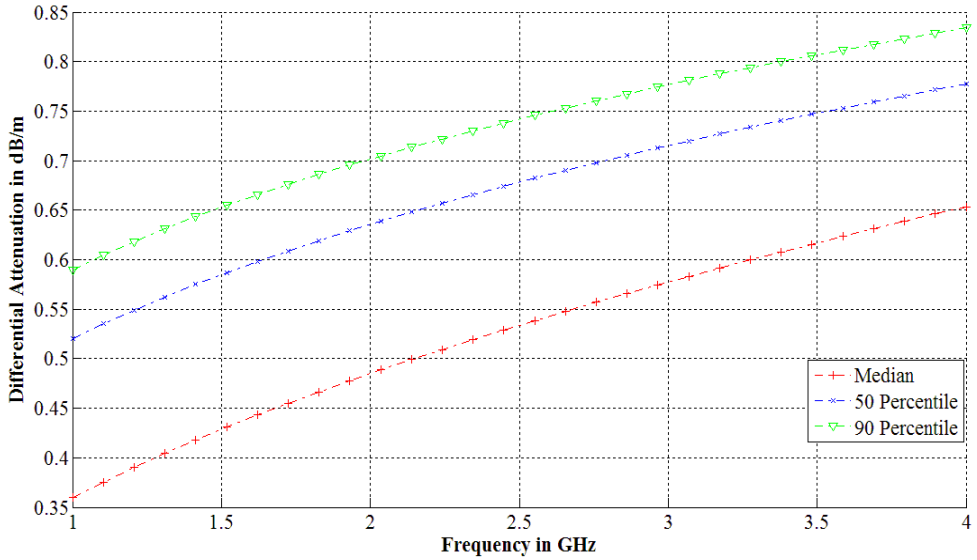

Figure 42. Differential attenuation versus frequency, tree without foliage (winter). (After [25])

2. Excess Path Loss Model for Two Single PRRs

The foliage distance at 70 m is chosen to coincide with the same communication range achievable during the field trial for the foliage scenario with an autonomous group in Section II.C.2.c. Figure 43 shows the scenario configuration. Figures 44 and 45 show the plot of excess path loss versus frequency in median, 50th percentile and 90th percentile with foliage distance d_{f_1}=70 m for summer and winter, respectively.

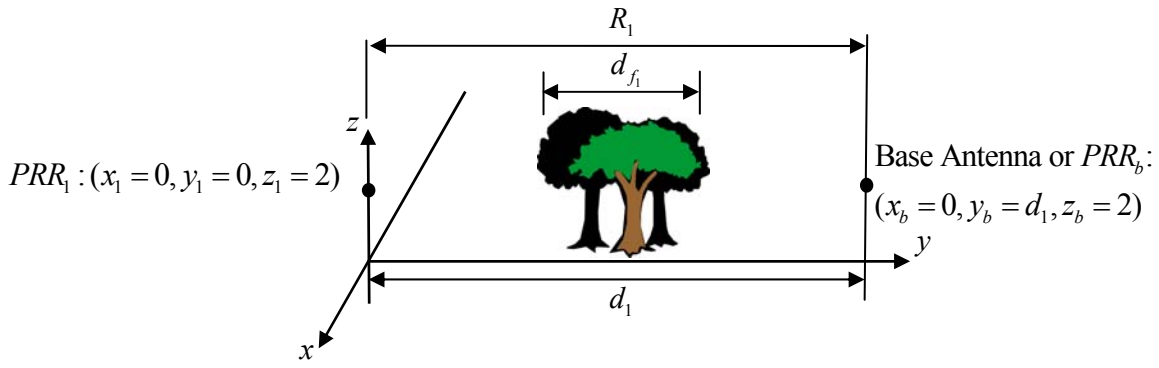

Figure 43. Single PRR configuration with PRR_1 at ($x_1 = 0, y_1 = q, z_1 = 2$) and receiving PRR_b at ($x_b = 0, y_b = d_1, z_b = 2$), and foliage distance at d_{f_1} in meters.

In Section III.C.2, it was determined that in order for successful communication to take place, the received power signal P_r threshold value according to manufacturer's specification at 800 m must be above –106.28 dBW. From Figure 16, the received powers P_r at distance 70 m is determined to be –85.12 dBW. Since the field trial was conducted in summer conditions, with the communication frequency at 2.45 GHz, the excess path loss is determined to be 18.79 dB from the 50th percentile plot in Figure 44. Summing the received power signal P_r and excess path loss at 70 meters gives –103.91 dBW which is fairly close to the determined threshold value of –106.28 dBW. The difference could be due to equipment tolerances, actual foliage distance rounding off, etc. Therefore, the foliage model can still be used to accurately predict the excess path loss due to foliage for other scenarios.

For the same scenario conducted during winter, the excess path loss is determined to be –16.74 dB at 50th percentile from Figure 45. Using Figure 16, the 2-dB difference between summer and winter excess path loss condition translates to about an additional 20 m of available communication range which represents an increase of 28.5% during winter foliage condition.

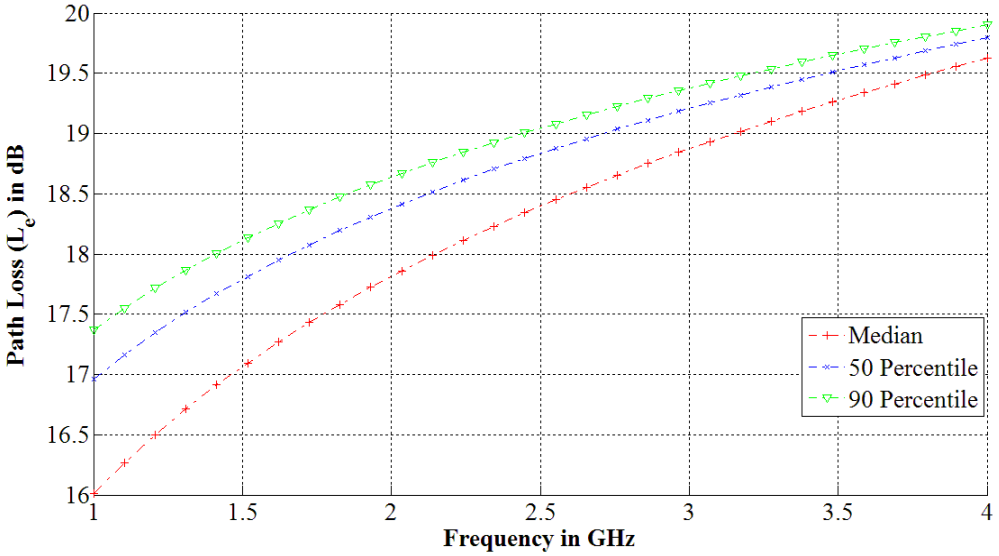

Figure 44. Excess path loss versus frequency, tree with foliage (summer).

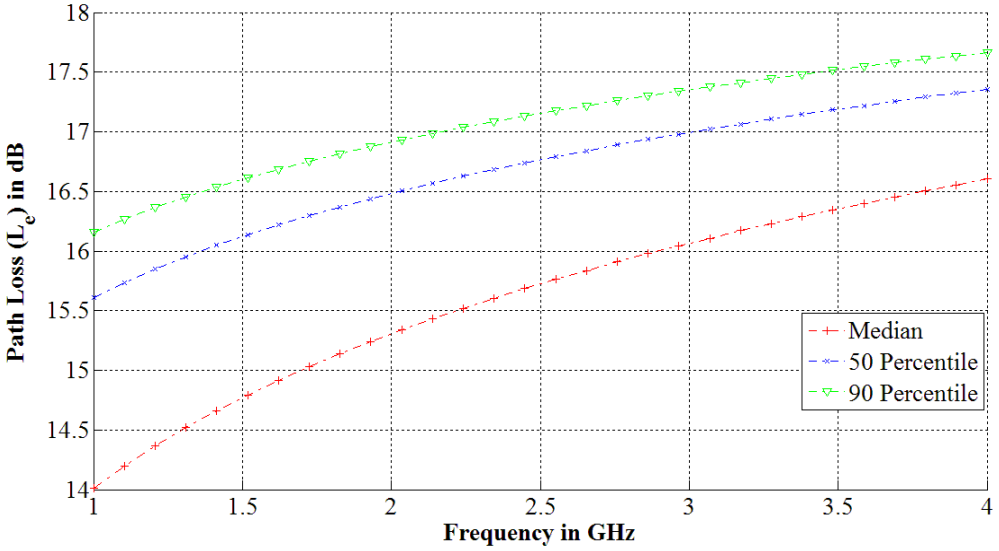

Figure 45. Excess path loss versus frequency, tree without foliage (winter).

3. Excess Path Loss Model with Beamforming Strategies

From the field trial report, operations conducted under foliage conditions degraded the communication range significantly. In Chapter III, PRRs using beamforming were shown to increase the communication range compared to a single PRR transmission. Assuming that the focused beam is always pointing accurately towards the intended receiver, the excess path loss effect on beamforming performance is analyzed. Figure 46 shows the scenario configuration.

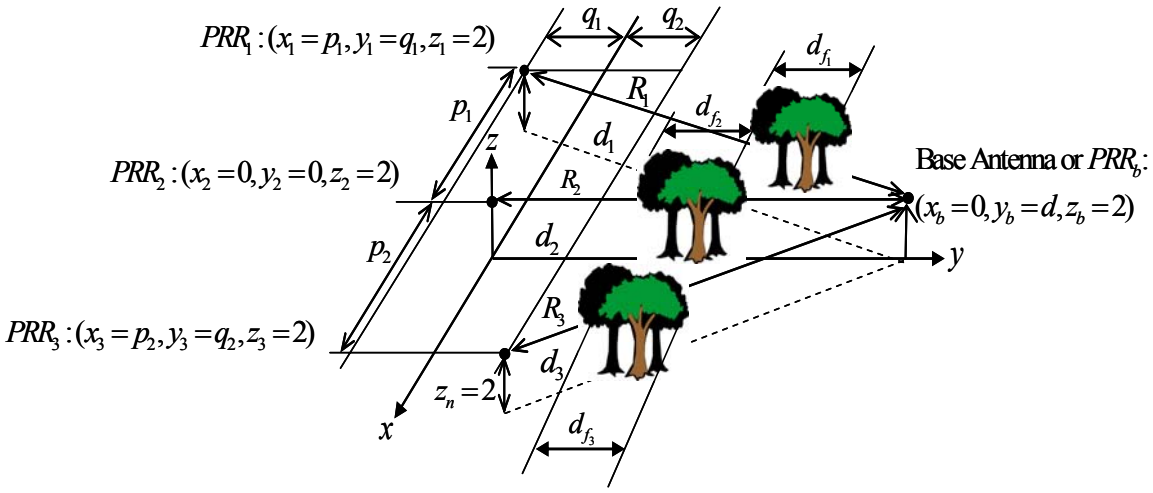

Figure 46. Three PRR configured with PRR_1 at $(x_1 = p_1, y_1 = q_1, z_1 = 2)$, PRR_2 at $(x_2 = 0, y_2 = 0, z_2 = 2)$ and PRR_3 at $(x_3 = p_2, y_3 = q_2, z_3 = 2)$, and receiving PRR_b at $(x_b = 0, y_b = d = d_2, z_b = 2)$,and foliage distances at d_{f_1}, d_{f_2} and d_{f_3} in meters.

a. Soldier Displacement Distances at 5 m apart, Range Distance at 800, and Foliage Distances at 70 m

Figure 47 shows the plot of the received power signal at focus range for three PRRs. From the plot, it can be seen that without foliage, the received power is –96.74 dBW. Without presence of foliage, communication is still possible as the received power is within the threshold value of –106.28 dBW. With 70 m of foliage, the received power of –113.5 dBW and –115.53 dB for winter and summer conditions at 800 m is below that of the threshold value of –106.28 dB for effective communication. There is a

loss of 16.79 dB and 18.79 dB due to foliage under winter and summer conditions. This shows that even with beamforming, the gains achieved cannot overcome the excess path loss due to foliage.

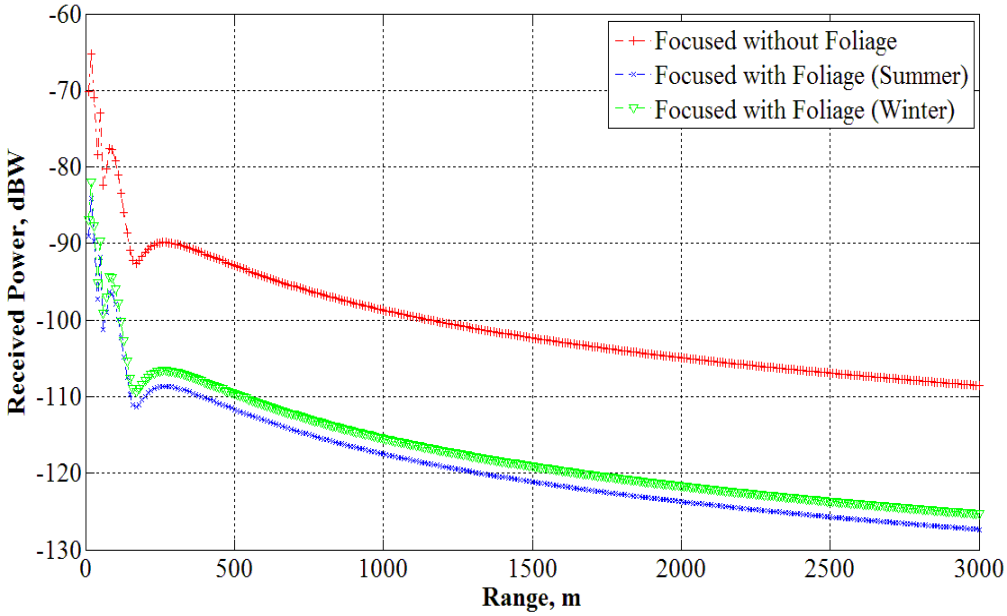

Figure 47. Plot of received power signal at focus range for three PRRs at range distance 800 m, displacement distances at 5 m and foliage distances at 70 m.

From Chapter III.C.3.a, with the implementation of beamforming, it can be seen that the strategies bring about an increase of 9.5 dB in terms of received power signal P_r. Figure 48 shows the plot of excess path loss versus foliage distance. From the plot, the 9.5-dB increase by employing beamforming strategy translates to only about 9 and 15 m in foliage distance for summer and winter conditions, respectively. For the extreme case where the threshold value of –106.28 dBW is used, this would provide an additional 3 dB to the 9.5 dB derived from beamforming thereby extending the communication range in foliage by another 20 and 50 m for summer and winter conditions, respectively. This amounts to 28.5% and 85% increase in communication range for summer and winter conditions, respectively.

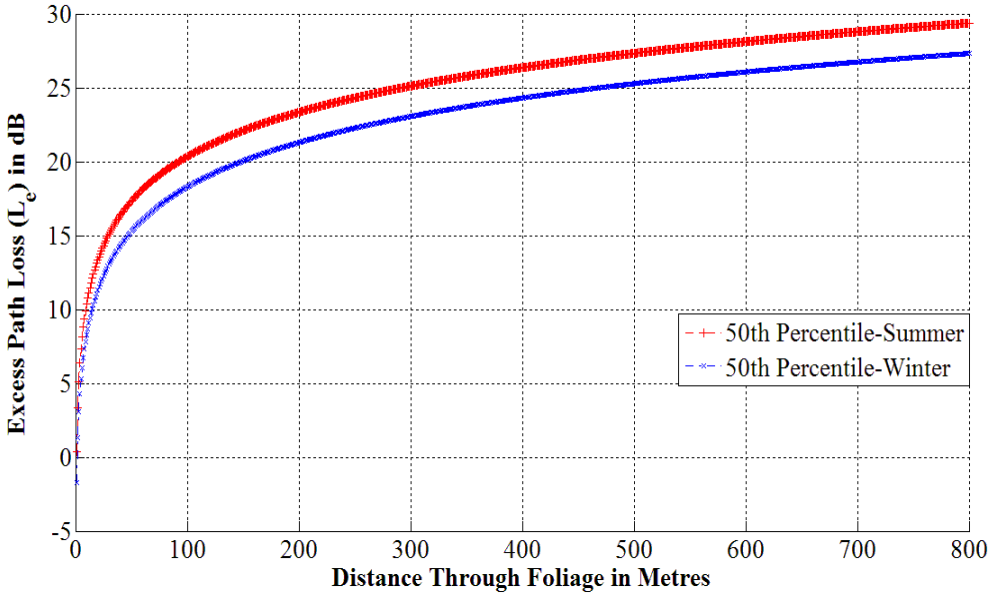

Figure 48. Excess path loss versus foliage distance (summer and winter).

The analysis performed so far assumed that all the PRR elements faced the same foliage conditions; thus the excess path loss is the same for all three elements. It would be interesting to look at various scenarios where the foliage distances are different for the three PRR elements and study the effects of foliage on beamforming performance.

b. Soldier Displacement Distances at 5 m apart, Range Distances at 800, and Foliage Distances at d_1=70, d_2=10 and d_3=10 m

Figure 49 shows the plot of the received power signal at focus range for three PRRs. With the different foliage distances, the received power becomes –107.8 dBW and –109.8 dBW for winter and summer conditions at 800 m which is also below that of the threshold value of –106.28 dBW for effective communication. There is a loss of 11.06 dB and 13.06 dB due to foliage under winter and summer conditions.

With these parameters, even with beamforming, the gains achieved cannot overcome the excess path loss due to foliage.

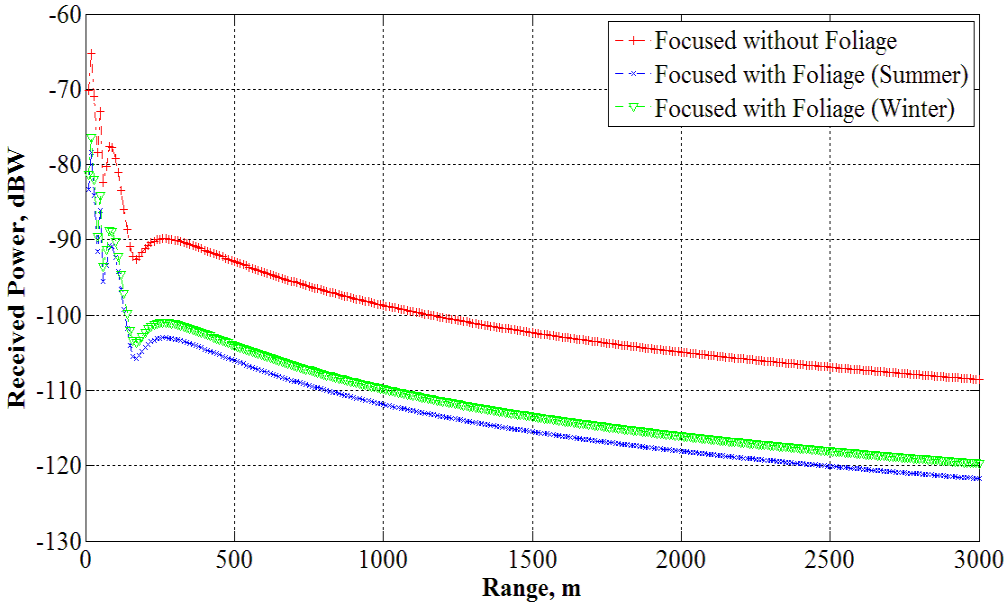

Figure 49. Plot of received power signal at focus range for three PRRs at range distance 800 m, displacement distances at 5 m and foliage distances at $d_{f_1} = 70, d_{f_2} = 10$ and $d_{f_3} = 10$ in meters

c. Soldier Displacement Distances at 5 m apart, Range Distances at 500, and Foliage Distances at d_1=70, d_2=10 and d_3=10 m

Figure 50 shows the plot of the received power at focus range for three PRRs. From the plot, the received power becomes –103.8 dBW and –105.8 dBW for winter and summer conditions at 500 m. The values are within the threshold value of –106.28 dBW for effective communication. There is a loss of 11.14 dB and 13.14 dB due to foliage under winter and summer conditions.

With the range distances at 500 m, and with improvement from beamforming, it is possible to overcome the excess path loss due to foliage.

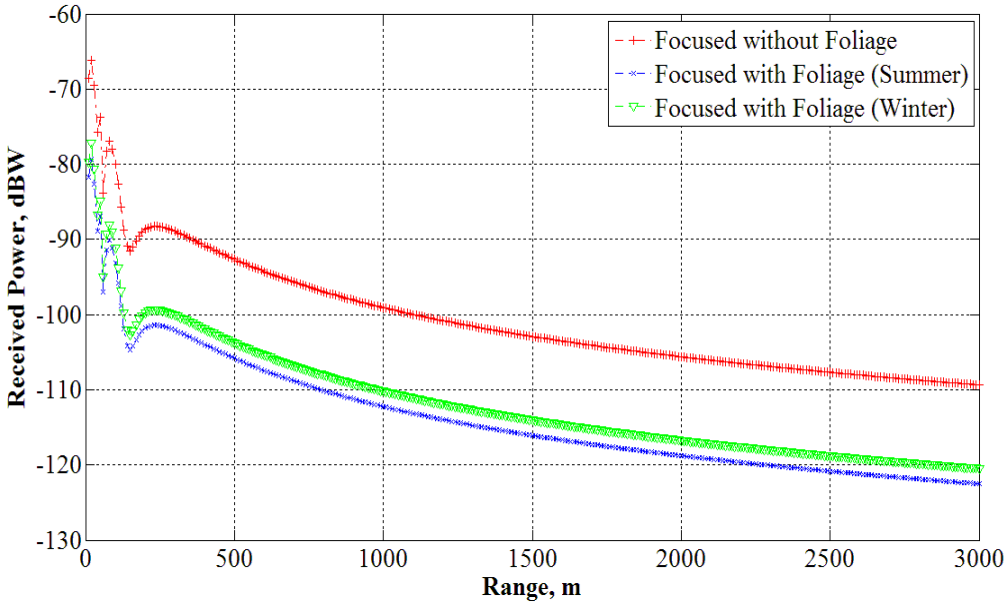

Figure 50. Plot of received power signal at focus range for three PRRs at range distance 500 m, displacement distances at 5 m and foliage distances at $d_{f_1} = 70, d_{f_2} = 10$ and $d_{f_3} = 10$ in meters

d. Soldier Displacement Distances at 5 m apart, Range Distances at d_1=505, d_2=500 and d_3=495 m, and Foliage Distances at d_1=70, d_2=10 and d_3=10 m

Figure 51 shows the plot of the received power at focus range for three PRRs. From the plot, the received power becomes –107.4 dBW and –109.4 dBW for winter and summer conditions at 500 m. The values are below the threshold value of –106.28 dBW for effective communication. There is a loss of 11.13 dB and 13.13 dB due to foliage under winter and summer conditions.

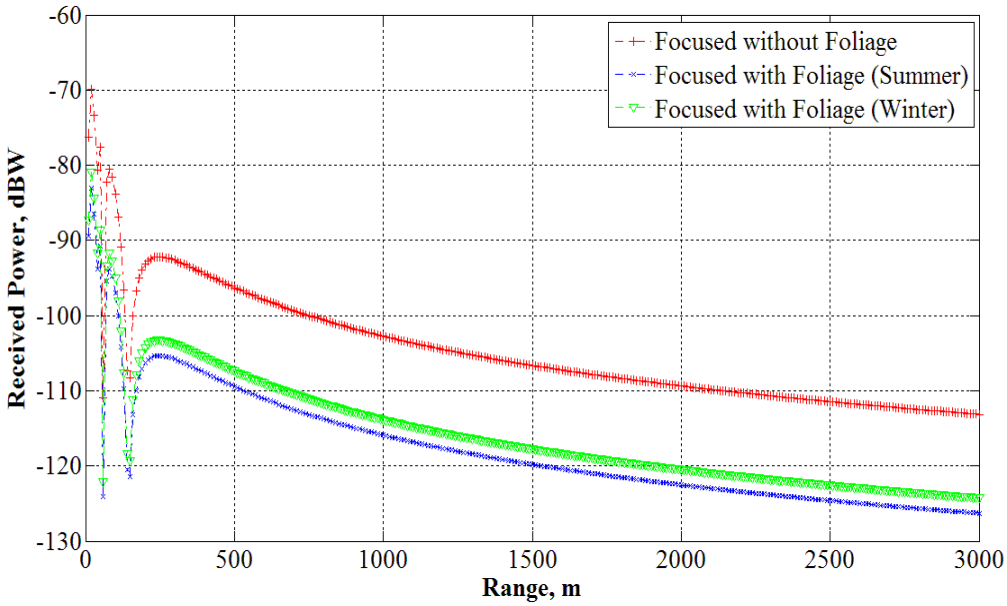

Figure 51. Plot of received power signal at focus range for three PRRs at range distance $d_1 = 505$, $d_2 = 500$, $d_3 = 495$ m, displacement distances at 5 m and foliage distances at $d_{f_1} = 70$, $d_{f_2} = 10$ and $d_{f_3} = 10$ in meters

D. SUMMARY

This chapter presented the foliage environment's effects on wave propagation. The rationale, considerations and assumptions on modeling of the foliage environment were described. The results of the Matlab simulation on the effects of a foliage environment and seasonal changes on the adopted beamforming strategies were analyzed. Findings showed the benefits gained from adopting beamforming strategies cannot overcome the effects of the foliage environment due to excess path loss in most of the cases, but still managed to show a significant increase in communication range.

The next chapter will look into the topic of synchronization for successful beamforming. The chapter will introduce and evaluate different synchronization methods. Analytical analysis on placement errors which lead to phase errors affecting the gains of the distributed beamforming will be performed. The simulation model and the analytical results will be presented, with results analyzed and discussed.

V. SYNCHRONIZATION FOR BEAMFORMING

This chapter begins by describing the concepts and importance of synchronization for efficient beamforming. Next, various methods of synchronization are evaluated and discussed. Following which, an analysis of placement errors, which translate to phase errors and therefore affect the gains achieved by distributed beamforming, is performed. Finally, simulation by Matlab on the analysis is performed, followed by discussion of the simulation results.

A. CONCEPTS OF SYNCHRONIZATION FOR BEAMFORMING

In Chapter III, distributed beamforming was shown to increase the range of communication in the PRR system. From the simulation results, the PRR elements were able to direct a beam in the desired direction. While the benefits of beamforming brought about an increase in terms of gains resulting in greater communication range, there is a cost associated with synchronizing and geolocating the PRR elements in order to achieve these gains. This cost depends not only on accurate knowledge of the channel, but also on time and phase synchronization at the transmitter. In practice perfect synchronization is not possible. The question is whether adequate synchronization is achievable so that the performance gains of cooperative beamforming can be obtained.

In a centralized beamforming operation, the baseband signals for all antenna elements are synchronized in time, and the carrier frequency and phase used to modulate the baseband signals are the same for all antenna elements. Similarly, for beamforming in a distributed manner, the key parameters for synchronization are carrier frequency and phase synchronization, and timing synchronization, among the distributed antenna elements. To achieve efficient distributed beamforming, the received carrier frequencies, the carrier phases, and the symbol timing of all propagated waves have to be the same when received by the receive antenna. As clocks are triggered by oscillators, the instantaneous phase of the oscillator of an antenna can be precisely determined by the time scale at the individual PRR antenna element. [2, 10, 28]

Much research has been conducted in the area of synchronization methods [8-10]. For the purpose of this research, the focus area is the general capabilities and limitations of the methods to evaluate how they might perform in the beamforming scenarios considered here. Specifically, the objective is to estimate the reduction in P_{r_b} that occurs when the synchronization is not perfect, and there are residual phase errors.

There are several approaches to synchronizing the PRRs. The PRRs do not have to be synchronized with the base station, although one possible technique is to use the base station as a master for synchronizing the PRRs. This approach is not considered because the base station may be out of range of the individual PRRs. Also the base station performs multiple tasks, not only with its local radios but also with other base stations. Synchronization would be time consuming and possibly degrade base station performance in other functions. Thus we are interested in methods that involve only the PRRs but not the base station.

Synchronization among the PRRs does not require that the radios know their locations. However, to focus the collective beam at the base station, the radios must know their location relative to the base station accurately. In order to bound the phase error due to placement error θ_e to within $\delta\theta$, where $\delta\theta$ implies that placement error distance $|d_e(n)| \le \lambda\,\delta\theta/2\pi$. Therefore, the smaller the carrier frequency, the less stringent the requirements on placement error for satisfying a desired phase synchronization tolerance. However, since the PRR carrier frequency is at 2.45 GHz, the tolerance on the placement error for a phase tolerance of 30^0 is extremely stringent: $|d_e| \le 10$ mm. This is about the best achievable by GPS in the most favorable conditions. Therefore, the placement error has to be small enough to permit accurate distributed beamforming.

Messages are sent simultaneously from all radios, and therefore all must share a common time reference. The ROVIS system employs the time division multiplex multiple access (TDMA) scheme. The TDMA channel is made up of 20 bits with data rate at 2.56 Mbps. Each TDMA channel is allocated a time 7.8125 μsec. The transmission time delay at range differences of 20 m is given by d/c, and calculated to be 67 ns. It can be seen that the additional propagation delay is small compared to the channel time

and thus can be neglected. The timing delay differences between radios may have to be compensated if the PRRs become widely spread.

B. METHODS OF SYNCHRONIZATION

There are two radio synchronization approaches to be considered: mutual synchronization and master-slave synchronization. The details of the techniques are given in numerous references [2, 28], so only a brief description is given here.

1. Mutual Synchronization Approach

With mutual synchronization and frequency, each clock collaborates with other clocks to determine the common time scale. Once the relative differences in time and phase are determined for all radios, compensation can be provided in the beamforming and waveform generation. This approach is preferred when no clock is superior to others and the robustness of the common time scale, with respect to the drift of any clock, is very critical. There are two disadvantages associated with this synchronization method. The first disadvantage is the significant overhead, which consumes time and energy, is required for clocks to determine the common clock scale. The second disadvantage is that a multiple access or coding scheme must be employed to differentiate one clock from the other.

2. Master-Slave Synchronization Approach

For the master-slave synchronization approach, since each slave clock is able to keep track of the variation of master clock accurately, the clock drift is no longer an issue. The master can be any designated PRR. Pre-compensation is required for each transmit antenna to compensate unequal propagation delays. In network synchronization, the propagation delays from the master clock to the slave clocks are compensated either in the master clock in advance or in the slave clocks afterwards. Therefore, at any point in time, all clocks have the same time scale. The waves are desired to arrive at the receive antenna coherently, which is similar to time requirements for the time division multiple access (TDMA) in satellite communications, where signals from transmit antennas must arrive at the satellite at specified time points. If the delays from all transmit antennas to

the receive antenna were the same, the consequence is just a shift of the time scale, and all signals could arrive coherently. However, because the delays are actually different, clocks in transmit antennas have to be pre-compensated to account for different propagation delays from the transmit antennas to the receive antenna. Thus, the delays from the master to the slave clocks have to be compensated, and the delays from the transmit antennas to the receive antenna must be pre-compensated. There are two types of methods for the combination of master-slave synchronization and pre-compensation. They are distinguished by whether a feedback loop is used at the slaves. [2, 28]

a. Open-Loop Master-Slave Synchronization

The first type is the open-loop approach. For a master-slave pair, both master and slave antennas transmit their clock scales to each other. Based on the clock scales of the incoming waves and the local antenna, the clock difference and pre-compensation are constantly calculated cooperatively by the master and the slave antenna. The slave clock accordingly updates its clock and pre-compensation by changing delay, while the master updated the pre-compensation only. The slave clock makes no effort to adjust its oscillator frequency in response to the clock difference. If the master and the slave oscillator frequencies are off by a large difference, the clock difference will increase rapidly after updates. This will result in poor synchronization or the need to re-synchronize frequently.

b. Closed-Loop Master-Slave Synchronization

The second type is the closed-loop approach. The slave clock is a voltage-controlled oscillator (VCO). The error signal is the clock difference mentioned above, and this signal is used to adjust the VCO frequency as opposed to the delay as in the open-loop approach. The problems with closed-loop approach are the stability and the tracking ability. Unlike ordinary phase lock loops, this loop includes two significant delays, one in the master-to-slave transmission and the other in the slave-to-master transmission. Since the delay is so huge, to keep the loop stable, the loop bandwidth must be narrow, and the tracking ability will be reduced.

A closed loop approach employs a VCO at the slave antenna to track the master clock frequency which is received at the slave antenna, and the phase comparison is done locally. Thus, the problem due to long propagation delay is avoided as in the closed-loop approach, while slave clocks can track the frequency of the master clock. This method is commonly used to extract the carrier from a received signal so that it can be used as a local oscillator reference. [29]

Compensation for the master-slave propagation delay is implemented jointly with pre-compensation for transmit-receive propagation delay as shown in Figure 52. The implemented TDMA scheme already adopted by the PRR system can be utilized to compensate slave clocks for the master-slave propagation delay with delay elements. This process can be combined with transmit-receive propagation delay pre-compensation since this procedure requires a lot of signaling to determine the amount of compensation. The clock of the transmit antenna can be a master or a slave clock. The time difference measured at the receive antenna is the sum of both propagation delays which are indistinguishable. This value is modulated, fed back, demodulated, and used in the single delay element.

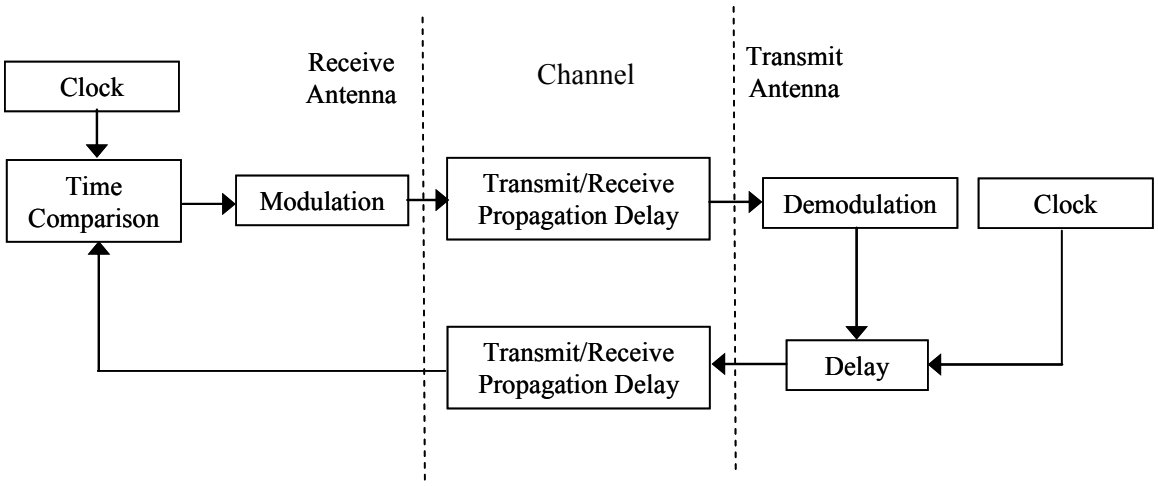

Figure 52. Compensation and pre-compensation. (After [2])

3. Beamforming in TDMA Systems

Co-channel interference and intersymbol interference (ISI) present problems in Time Division Multiplexing (TDM) and Time Division Multiple Access (TDMA) communication systems. As transmission resources become more congested those problems will become more prevalent. Beamforming can be used to improve the situation. The signal environment is often time varying so adaptive compensation techniques should be employed. Use of a beamformer-demodulator to extract co-channel TDMA signals and compensate for ISI can significantly increase system capacity by allowing more reuse of the same RF channels in a geographic area.

At each transmit antenna, both information and synchronization signals are transmitted. The two signals are multiplexed in the time domain, while the timing and phase reference are shared. Data signals from all transmit antennas occupied the same channel in the time domain. Information signals are therefore received at the receive antenna coherently.

C. SYNCHRONIZATION ANALYSIS

Both synchronization error and position errors lead to a phase error that reduces the received power from the ideal case. In this section both are treated as random errors with similar behavior. In [10], the study determined how placement errors affect the gains achieved by distributed beamforming.

Three trends were noted in the study:

1. $P_{r_b} / N \to E\left[\cos(\theta_f)\right]$ converged as $N \to \infty$, where θ_f is -2 θ_e and θ_e is the phase error resulting from placement error; $E[.]$ denotes expected value. When the total transmit power is kept constant, the received signal power increases linearly with N as N tends to ∞.

2. For finite N,

$$E[P_r] = 1 + (N-1)\beta_\theta^2 \tag{5-1}$$

where $\beta_\theta = E[\cos(\theta_f)]^2$. Therefore, even for finite N, the expected value of the received signal power increases linearly with N.

3. When N is large enough for the central limit theorem to apply,

$$P_{r_b} \approx X_c^2 + X_s^2 \tag{5-2}$$

where $X_c \sim N(m_c, \sigma_c^2)$, $X_s \sim N(0, \sigma_s^2)$ and the parameters m_c, σ_c^2, and σ_s^2 are given as follows:

$$m_c = \sqrt{N} E[\cos(\theta_f)] \tag{5-3}$$

$$\sigma_c^2 = 2E[\cos^2(\theta_f)] - E[\cos(\theta_f)]^2 \tag{5-4}$$

$$\sigma_s^2 = 2E[\sin^2(\theta_f)] \tag{5-5}$$

The variance of the received signal power is then

$$\text{var}[P_r] = 4\sigma_c^2 m_c^2 + 2\sigma_c^4 + 2\sigma_s^4 \tag{5-6}$$

which increases linearly with N. When there are no phase errors, Equation (5-6) reduces to

$$\text{var}[P_r] = 4N \tag{5-7}$$

The study found that:

1. The expected value of P_{r_b} increases as $\beta_\theta N$, where β_θ is a function of the phase error distribution and $0 \le \beta_\theta \le 1$. When there is no phase error, $E[P_r] = N$, meaning that beamforming with *N* PRR elements gives a power gain of *N* over transmission with a single PRR element as noted in Equation (3-34). Thus, the degradation caused by phase errors is contained in the term β_θ.

2. The variance of P_{r_b} also increases linearly with *N*, for both zero and nonzero phase errors. The existence of phase errors increases the variance over that of an ideal, error-free system. Therefore, as long as the distribution of placement errors is contained, keeping β_θ close to 1, large gains can still be realized using distributed beamforming.

D. MATLAB SIMULATION

Using uniform distribution for the phase errors $\theta_f \sim U[-\pi\Delta, \pi\Delta]$ where $0 \le \Delta \le 1$ and using the approximation $\cos(\theta) \cong 1 - \theta^2/2$ and Equation (5-1) gives

$$E[P_r] = 1 + (N-1)\left(1 - \frac{1}{6}(\pi\Delta)^2\right)^2 \tag{5-8}$$

where $\Delta = 0.1$ corresponds to a placement error spread of 0.05λ, $\Delta = 0.2$ corresponds to a placement error spread of 0.1λ, etc.

Figure 53 shows the plot of normalized expected value of received power P_{r_b} versus number of PRR elements, *N*. From the plot, it can be seen that the normalized expected value of received power is still high at 0.968 and 0.875 even with a placement error of $\Delta = 2$ and $\Delta = 4$ at one and two wavelengths, respectively for three PRR elements. However, the expected value of received power degrades rapidly at $\Delta = 8$ with only 0.58 power received.

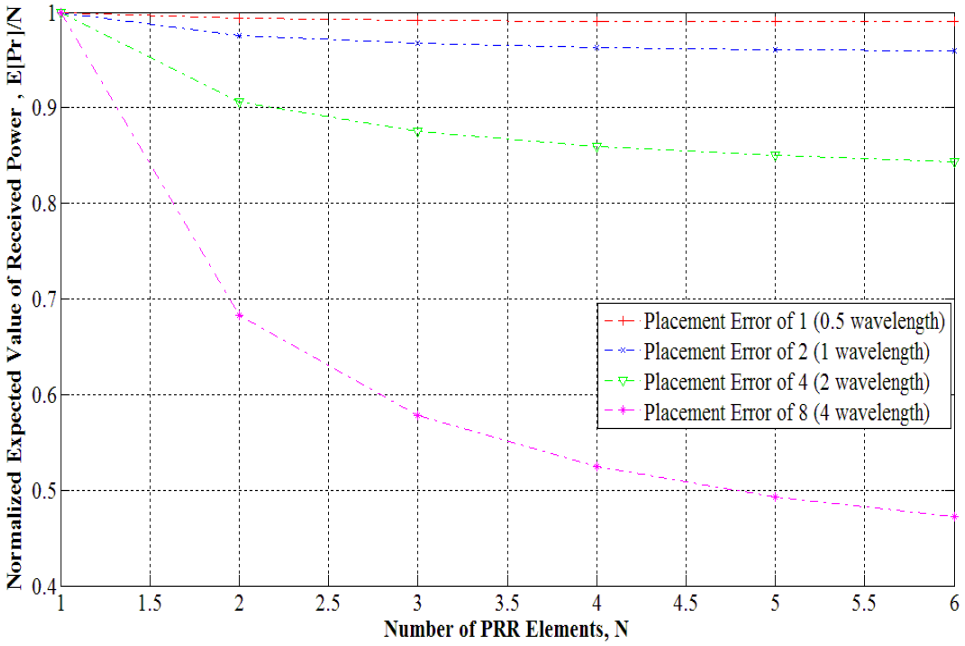

Figure 53. Plot of normalized expected value of received power $E[P_r]/N$ versus number of PRR elements, N. (After [10])

Figure 54 shows how the expected value of received power scales with PRR elements for different placement errors values. A maximum slope of 1 corresponds to the case of ideal beamforming. For $\Delta = 8$ and $N = 3$, there is a 42% loss compared to the ideal benchmark of 3. However, the expected value of the received power is still 1.7 times that for a single antenna transmission. For the extreme case of $\Delta = 8$ and $N = 30$ (maximum number of users), there is a 60% loss compared to the ideal benchmark. Nevertheless, the expected value of received power is still 12 times that for a single antenna transmission.

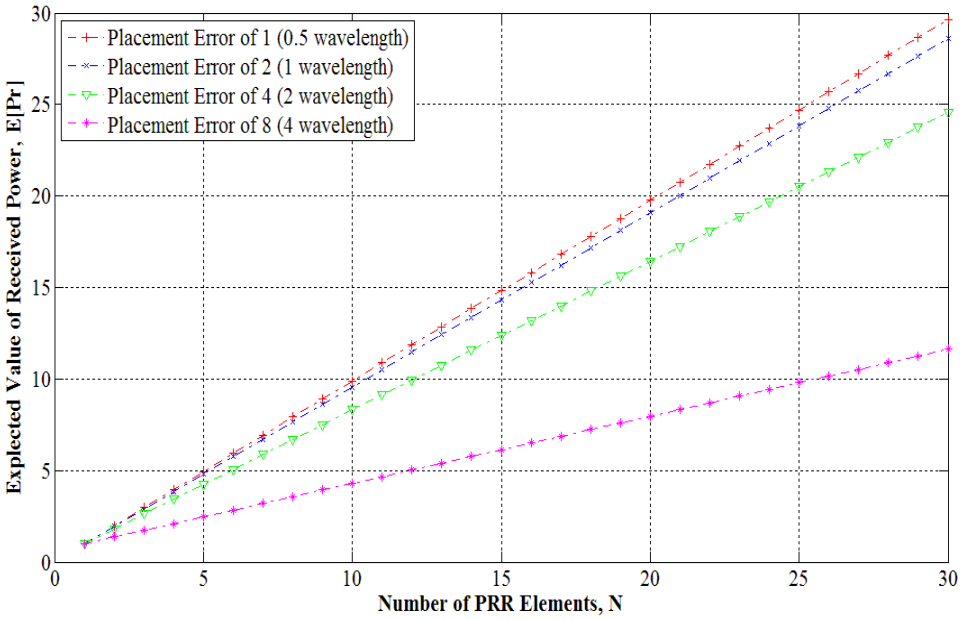

Figure 54. Plot of expected value of received power $E[P_r]$ versus number of PRR elements N. (After [10])

To consider how the variance of P_r scales with N, the approximations of $\cos(\theta) \cong \theta - \theta^2/2$ and $\sin(\theta) \cong 1 - \theta^3/6$ are used. If phase errors are uniformly distributed where $\theta_f \sim U[-\pi\Delta, \pi\Delta]$, the Equations (5-3) to (5-5) can be expressed as

$$m_c = \sqrt{N}\left(1 - \frac{\pi\Delta}{6}\right) \tag{5-9}$$

$$\sigma_c^{\,2} = 1 - \frac{(\pi\Delta)^2}{3} + \frac{13(\pi\Delta)^4}{180} \tag{5-10}$$

$$\sigma_s^{\,2} = \frac{2(\pi\Delta)^2}{3} - \frac{2(\pi\Delta)^4}{15} + \frac{(\pi\Delta)^6}{126} \tag{5-11}$$

The variance of P_r can be calculated using Equation (5-6). Figure 55 shows the plot of variance of the received power versus number of PRR elements for various values of placement errors.

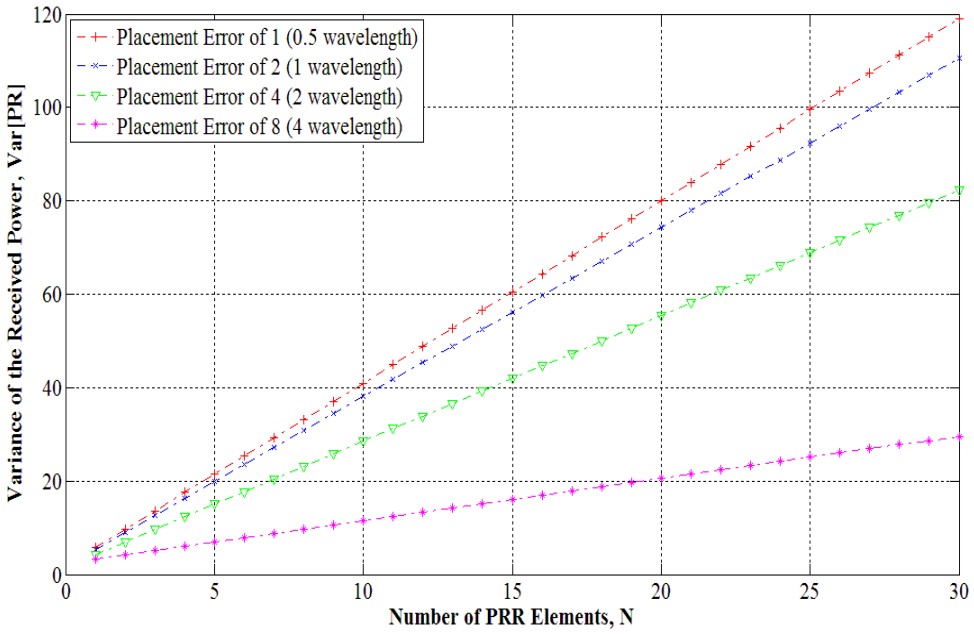

Figure 55. Plot of variance of the received power $\mathrm{Var}[P_r]$ versus number of PRR elements, N. (After [10])

From the plot, for $\Delta = 8$ and $N = 3$, there is a 60% loss compared to the ideal benchmark of 13.66. However, the variance of received power is still 1.53 times that for a single antenna transmission. For the extreme case of $\Delta = 8$ and $N = 30$ (maximum number of users), there is a 75% loss compared to the ideal benchmark, but is still 8.8 times that for a single antenna transmission.

E. SUMMARY

This chapter presented the concepts and importance of synchronization for efficient beamforming. Next, various methods of synchronization were presented and discussed. Following which, an analysis of placement errors affecting the gains achieved by distributed beamforming is performed. Finally, simulation by Matlab on analysis results were performed, with the results presented and discussed.

The following chapter presents the conclusions for this thesis and offers a few topics for possible future work.

THIS PAGE INTENTIONALLY LEFT BLANK

VI. CONCLUSIONS AND FUTURE WORK

A. SUMMARY

The research objective was to examine networked "man portable" wireless communication networks in a non-ideal operating environment such as in foliage terrain and to determine if cooperative beamforming can improve performance. The soldier communication network studied in this research is based on CWICS 200 communication system from COBHAM Defence Communication. Field trials of various scenarios and corresponding performance of the system were presented and utilized throughout the study.

Some concepts in distributed beamforming were presented and discussed. Different PRR system configurations under field operating scenarios were modeled in Matlab. Two baseline models were used for reference: (1) a link between a single PRR and a vehicle antenna, and (2) a link between two PRRs. The results were used as a baseline for comparison with other models. The benefits and limitations of beamforming for the different scenarios were discussed.

Seasonal foliage effects on the wireless network were considered in the study. The foliage environment's effects on wave propagation were presented. The rationale, considerations and assumptions in modeling of the foliage environment were described. The results of Matlab simulation on the effects of foliage environment and seasonal changes on the adopted beamforming strategies were analyzed.

Using distributed beamforming techniques in wireless networks, the communication range can be increased to overcome foliage attenuation and other losses. While the benefits of beamforming brought about an increase in terms of gains resulting in greater communication range, there is a cost associated with synchronizing the PRR elements in order to achieve these gains. This cost depends not only on accurate knowledge of the channel, but also on time and phase synchronization at the transmitter. Finally, analysis of placement errors which translate to phase errors affecting the gains achieved by distributed beamforming was performed and loss curves calculated.

B. CONCLUSION

The results and data analysis from the Matlab simulations for the distributed beamforming have shown that practically beamforming can most likely only be applied for short displacements between the soldiers for accurate focusing at the location of the vehicle base station or a PRR element in another operating unit. For three PRR elements, there is a gain increase of 9.5 dB in the received power. However, due to the extremely short wavelength, the achievable half power beam width is less than 1 degree, and for this reason it is difficult to focus the beam at the base station.

The Matlab simulation results based on a specific foliage environment and seasonal change model showed that the benefits gained from the adopted beamforming strategies cannot completely overcome the effects of the foliage environment due to excess path loss but still managed to show a significant increase in communication range. Improvements on the order of 28.5% and 85% increase in communication range for summer and winter conditions are still achievable with beamforming.

Finally, analysis of placement errors, which translate to phase errors, affect the gains achieved by distributed beamforming. With a uniformly distributed placement error of $\Delta = 8$ (4 wavelengths) and beamforming using 3 PRR elements, there is a 42% loss from the expected value of received power and 60% loss for the variance for the received power relative to the error-free case. However, the expected value of received power is still 1.7 times and the variance of the received power is still 1.53 times than that for a single antenna transmission. For the extreme case of a placement error of $\Delta = 8$ with 30 PRR elements (maximum number of users), there is a 60% loss of expected value of received power and 75% loss for the variance of the received power. Nevertheless, the expected value of the received power is still 12 times and the variance of the received power is still 8.8 times that of a single antenna transmission.

Effective cooperative beamforming relies on all elements being synchronized and accurate knowledge of their locations relative to the base station so that the beam can be focused. In a practical operational system this will be very difficult to accomplish.

C. FUTURE WORK

In the distributed beamforming study in the thesis, the PRR elements and vehicle base station locations are assumed fixed (not moving). Beamforming performance will be affected by any changes in the locations of the PRR elements and vehicle base station, since the wavelength is small due to the high carrier frequency (upper UHF band). In addition, the issues of multipath, fading and jamming are not dealt with in this study. Future work can include the dynamic consideration of the PRR elements and base station when the soldiers and vehicle are in motion to study the impact on distributed beamforming performance and look into the issues of multipath, fading and jamming. For the seasonal foliage effects model, only the coherent power of the signal was considered while the diffuse power from the field fluctuation was neglected. Future work may consider including the diffuse power for long-distance beamforming.

For the placement error analytical study, various assumptions were made such as the timing error is considered small since the range differences considered between PRRs were up to 20 m only. Future works will need to take into consideration if the timing error is large for longer displacement distances.

THIS PAGE INTENTIONALLY LEFT BLANK

LIST OF REFERENCES

[1] Trials Report, "ROVIS Wireless Intercom Extensions for SAF Armoured Vehicles," Chelton Defence Communication, June 2005.

[2] Y.S. Tu, and G.J. Pottie, "Coherent Cooperative Transmission from Multiple Adjacent Antenna To a Distant Stationary Antenna Through AWGN Channels," *IEEE 55th Vehicular Technology Conference,* Vol. 1, pp. 130-134, May 2002.

[3] D. Jenn, , Y. Loke, M. Tong, E.C. Yeo, C.S. Ong, and S.Y. Yeo, "Distrinuted Phase Arrays and Wireless Beamforming Networks," Naval Postgraduate School, 2007 (unpublished).

[4] B.D. Steinberg, *Microwave Imaging with Large Antenna Arrays: Radio Camera Principles and Techniques*, Wiley, 1983.

[5] E. Lee, and C.N. Dorny, "A Broadcast Reference Technique for Self-Calibrating of Large Antenna Phased Arrays," *IEEE Trans. on Antennas and Prop*., Vol. 37, No. 8, August 1989.

[6] G. Galati, and G. Losquadro, "Distributed-Array Radar System Comprising an Array of Interconnected Elementary Satellites," United States Patent Number 4,843,397, June 27, 1989.

[7] R. Hermiller, J. Belyea, and P. Tomlinson, "Distributed Array Radar," *IEEE Trans. on Aerospace and Elect. Systems*, Vol. AES-19, No. 6, Nov. 1983, pp. 831– 839.

[8] H. Ochiai, P. Mitran, H.V. Poor, and V. Tarokh, "Collaborative beamforming for distributed wireless ad hoc sensor networks," *IEEE Transactions on Signal Processing Workshop*, Vol. 53, No. 11, pp. 4110-4124, November 2005.

[9] R. Mudumbai, G. Barriac, and U. Madhow, "On the Feasibility of Distributed Beamforming in Wireless Networks," *IEEE Transactions on Wireless Communications*, Vol. 6, Issue 5, pp. 1754-1763, May 2007.

[10] R. Mudumbai, G. Barriac, and U. Madhow, "Distributed Beamforming for Information Transfer in Sensor Networks," in *Third International Symposium on Information Processing in Sensor Networks*, IPSN 2004, pp. 81-88, April 2004.

[11] M.E. Andersen , *How Col. John Boyd Beat the Generals*. http://www.insightmag.com/news/2002/09/02/National/How-Col.John.Boyd.Beat.The.Generals-260509.shtml. Posted on 12 August 2002.

[12] Cobham Defence Communiations, Medium and Heavy Vehicle Systems - AN/VIC-3 and ROVIS. http://www.cobhamdcweb.com/cdci/html/products/wirelesscommunications.htm. Last accessed 08 October 2007

[13] C.V. Chung, "Simulation of Radiowave Propagation in a Dense Urban Environment," Master's Thesis, Naval Postgraduate School, Monterey, March 2007.

[14] P. Vincent, "Energy Conversation in Wireless Sensor Networks," Dissertation Proposal, Naval Postgraduate School, March 2007.

[15] T.F. Ulaby, *Fundamentals of Applied Electromagnetics,* Media Edition, Prentice Hall Upper Saddle River, New Jersey, 2004.

[16] W.L. Stutzman, and G.A. Thiele, *Antenna Theory and Design*, Second Edition, Wiley, New Jersey, 1998.

[17] D.C. Jenn, Handwritten Notes, Naval Postgraduate School, 2007 (unpublished).

[18] J. Kraus, *Antennas*, McGraw-Hill, 1950.

[19] F. Wang, and K. Sarabandi, "A Physics-Based Statistical Model for Wave Propagation Through Foliage," *IEEE Transactions on Antennas and Propagation*, Vol. 55, Issue. 3 Part-2, pp. 958-968

[20] B. Benzair, H. Smith, and J.R. Norbury, "Tree attenuation measurements at 1-4 GHz for mobile radio systems," *Sixth International Conference on Mobile Radio and Personal Communications*, pp. 16-20, December 1991.

[21] F. Wang, I. Koh, K. Sarabandi, "Long distance path-loss estimation for wave propagation through a forested environment," *IEEE Antennas and Propagation Society International Symposium*, Vol. 1, pp. 922-925, June 2004.

[22] H.L. Bertoni, *Radio Propagation for Modern Wireless Systems*, Prentice Hall, New Jersey, 2000.

[23] W.J. Vogel, and J. Goldhirsh, "Tree attenuation at 869 MHz derived from remotely piloted aircraft measurements," *IEEE Transactions on Antennas Propagation*, Vol. 34, Issue. 12, pp. 1460-1464, December 1986.

[24] M.O. Nuaimi, and A.M. Hammoudeh, "Measurements and predictions of attenuation and scatter of microwave signals by trees," *IEE Proceedings on Microwave, Antennas and Propagation*, Vol. 141, pp. 70-76, April 1994.

[25] K. Benzair, "Measurements and modeling of propagation losses through vegetation at 1-4GHz," *Ninth International Conference on Antennas and Propagation*, Vol. 2, pp. 54-59, April 1995.

[26] Deciduous Tree Pictures. www.ppgn.com/dpic3.html. Last accessed 10 October 2007.

[27] Angie Horticulture Networks on Deciduous Trees. http://aggie-horticulture.tamu.edu/ornamentals/natives/trees/zanthoxych1844.jpg. Last accessed 10 Oct. 2007.

[28] V. Tarokh, S.C. Yang, and S. Alamouti, "Complementary beamforming," *IEEE 58th Vehicular Technology Conference*, Vol. 5, pp. 3136-3140, October 2003.

[29] J.B. Anderson, Digital Transmission Engineering, 2nd Edition, IEEE Press, 2005.

INITIAL DISTRIBUTION LIST

1. Defense Technical Information Center
   Ft. Belvoir, Virginia

2. Dudley Knox Library
   Naval Postgraduate School
   Monterey, California

3. Chairman, Department of Electrical and Computer Engineering, Code EC
   Naval Postgraduate School
   Monterey, California

4. Professor David Jenn, Code EC/Jn
   Department of Electrical and Computer Engineering
   Naval Postgraduate School
   Monterey, California

5. Professor Murali Tummala, Code EC/Tu
   Department of Electrical and Computer Engineering
   Naval Postgraduate School
   Monterey, California

6. Chan, Chun Man
   Singapore Technologies Engineering Ltd.
   Singapore